Title

Reinforced concrete wall buildings with force-limiting connections: Modeling effects and uncertainty propagation

Authors

Mayorga, C Franco

Tsampras, Georgios

Publication Date

2024-01-08

DOI

10.1002/eqe.4073

Received: 20 September 2023 | Revised: 14 December 2023 | Accepted: 15 December 2023

DOI: 10.1002/eqe.4073

RESEARCH ARTICLE

WILEY

Reinforced concrete wall buildings with force-limiting connections: Modeling effects and uncertainty propagation

C. Franco Mayorga | **Georgios Tsampras**

Department of Structural Engineering, University of California, San Diego, California, USA

Correspondence
C. Franco Mayorga, 9500 Gilman Dr., La Jolla, CA 92093, USA.
Email: cfmayorg@ucsd.edu

Funding information
Chilean National Agency for Research and Development (ANID)

Abstract

This paper assesses the effects of (1) the gravity load-resisting system (GLRS) modeling approach, (2) the seismic force-resisting system (SFRS) modeling approach, and (3) the uncertainty of the model parameters of the constitutive law of the longitudinal reinforcing steel of the SFRS on the seismic responses of a 12-story reinforced concrete wall building with force-limiting connections. This is achieved by conducting nonlinear numerical earthquake simulations. The seismic responses of the building models with force-limiting connections using two GLRS modeling approaches, (1) a moment frame system and (2) a pin-base lean-on-column system, are compared. The seismic responses of the building models with conventional connections and force-limiting connections, respectively, using two SFRS modeling approaches, (1) a distributed-plasticity modeling approach and (2) a lumped-plasticity modeling approach, are compared. A joint probability density function for the ASTM-A615 Grade 60 steel available in the literature is used to conduct an uncertainty propagation analysis through Monte Carlo simulation. The uncertainty in the steel model parameters is propagated to the seismic responses of the building models with conventional connections and force-limiting connections, respectively. The distributions of the mean values of the peak structural responses of the building models are studied. The effects of the GLRS modeling approach on the seismic responses are not significant in the context of seismic performance-based design and assessment of buildings with force-limiting connections. The effects of the SFRS modeling approach and the uncertainty in the steel model parameters on the floor total acceleration and force responses are reduced by including force-limiting connections.

KEYWORDS
force-limiting deformable connections, nonlinear numerical earthquake simulation, numerical modeling effects, reinforced-concrete wall buildings, uncertainty propagation

1 | INTRODUCTION

Numerical models are required to simulate the seismic responses (e.g., story shear, inter-story drift, acceleration, and local strain responses) of buildings subjected to ground motions generated by seismic events. These simulated responses are used to design new buildings or assess existing buildings. The assumptions associated with the modeling approaches affect the accuracy and the variability of the seismic responses computed numerically. Hence, the selection of the modeling approaches can affect the design and assessment of buildings. Furthermore, the seismic responses of some building systems may be more susceptible to the modeling approaches used to simulate the seismic responses of their structural components. In general, the suitability of the modeling approaches depends on the structural components of the building (e.g., beams, columns, walls, slabs, and seismic protection devices), seismic responses of interest, ground motion characteristics, computational cost, and desired level of accuracy. Therefore, the effects of the modeling approaches of the building structural components on the seismic responses of buildings have to be assessed. This is especially important during the development of high-performance non-conventional earthquake-resistant buildings with accelerated post-earthquake functional recovery.

1.1 | Numerical models proposed in the literature

Numerical models of the building structural components with different theoretical basis, complexity, and capability of prediction have been proposed and implemented to simulate the seismic nonlinear responses of buildings. It has been possible thanks to the progressive development of computational tools and the availability of experimental test results needed to validate the numerical models. The numerical models used to simulate the seismic nonlinear responses of the building structural components can be based on either linear-elastic, lumped-plasticity, macro-model, distributed-plasticity, or continuum modeling approaches. They can be defined either by force-deformation, moment-rotation, or stress-strain constitutive laws and consider either coupled or uncoupled axial, flexural, and shear responses.[1–5] The capability of the numerical models to predict the seismic structural responses of buildings depends on the complexity of the building (e.g., material properties, geometry, number of stories, and dynamic properties), the characteristics of the ground motion (e.g., intensity, frequency content, directionality, and duration), the assumptions made for the development of a modeling approach (e.g., nonlinearity, coupled structural responses, and modeled failure mechanisms), and the calibration of the numerical model parameters considering their uncertainty.[6,7] A comparative analysis is needed to select the appropriate modeling approach for the problem that is being solved. As an example, Belleti et al.[8] implemented lumped-plasticity, distributed-plasticity, and shell (macro model) modeling approaches of reinforced concrete (RC) structural walls for pushover analyses to assess their applicability for buildings with non-rectangular RC precast structural walls. This analysis allowed the authors to determine the most suitable modeling approach for the estimation of seismic responses computed using pushover analyses considering different levels of accuracy. They concluded that the lumped-plasticity modeling approach gives reliable results for rectangular and nonrectangular wall cross-section shapes. As another example, Pozo et al.[9] assessed the effects of the modeling parameters and discretization on the global and local nonlinear behaviors and computational times of numerical cyclic lateral force-deformation responses of squad and slender RC walls modeled using four nonlinear macro models. They proposed a new quantitative assessment approach of nonlinear macro models used to simulate the hysteretic responses of RC walls that can be incorporated into the performance-based seismic design guidelines for RC wall buildings. The same authors also conducted numerical earthquake simulations of RC wall buildings to quantify the effects of the variability from different nonlinear RC wall modeling approaches on the local and global responses using four fiber-based nonlinear models.[7] They concluded that the variability in the simulated global responses was significantly smaller than the variability in the simulated local responses. Another example of the suitability of numerical models is the implementation of the three-dimensional beam-truss model (macro model) proposed by Lu et al.[10,11] This model can simulate the nonlinear flexure-shear interaction of RC structural components (walls, slabs, and beams) and failure modes such as bar buckling, bar rupture, and concrete crushing. Mavros et al.[12] implemented a fully nonlinear numerical model of a 14-story RC core wall building using the three-dimensional beam-truss model. The building model was subjected to nonlinear cyclic-static lateral loading. They observed that the damage pattern and failure were governed by the nonlinear flexure-shear interaction in the wall piers, a considerable contribution of the compression flanges in the overall story-shear resistance, and a non-negligible effect of modeling the out-of-plane shear capacity of flanges. These nonlinear responses cannot be captured by other numerical models such as models based on the lumped-plasticity modeling approach. However, this sophisticated modeling approach may be impractical for analyses

that require a large number of numerical earthquake simulations (e.g., uncertainty propagation and reliability analyses) for the development of new structural systems with accelerated post-earthquake functional recovery. The definition of the suitable numerical models of the building's structural components requires conducting comparative analyses of the possible modeling approaches.

1.2 | Conventional earthquake-resistant buildings

Earthquake-resistant buildings are typically composed of two connected systems, a laterally flexible gravity load-resisting system (GLRS) and a laterally stiff seismic force-resisting system (SFRS). The GLRS transfers the vertical loads from the floors to the foundations. The SFRS resists the seismic-induced horizontal inertial forces developed by the acceleration of the mass distributed in the GLRS. Structural connections transfer the seismic-induced horizontal inertial forces from the GLRS to the SFRS. Conventional connections between the GLRS and the SFRS are stiff in the horizontal direction. Assuming the restoring and damping forces in the GLRS at a time instant of peak displacements are negligible compared to the inertial forces, the connection forces can be assumed equal to the inertial forces. Under this assumption, the connection forces are expected to be large and uncontrolled when the inertial forces are large. Large or even moderate inertial forces potentially lead to structural damage in the SFRS and the GLRS.[13–15] This potential structural damage can be reduced by including special connections between the GLRS and the SFRS.[16]

1.3 | Buildings with force-limiting deformable connections

The magnitude and variability of the inertial forces and the floor total accelerations can be limited by controlling the connection forces transferred between the GLRS and the SFRS.[16–23] This can be achieved by the design of connections that limit the forces transferred between the GLRS and the SFRS while allowing relative motion between these two systems. Tsampras et al.[16] developed force-limiting deformable connections that consist of two components: (1) a limited-strength hysteretic component to limit the forces transferred through the connections, and (2) a bearing component to provide post-elastic stiffness to prevent excessive inelastic deformation in the connections and provide the out-of-plane stability to the SFRS composed of planar structural elements. Figure 1 shows a schematic representation of the three-dimensional view, plan view, and connections between the GLRS and the SFRS of a building with force-limiting connections. This figure indicates the locations where the limited-strength hysteretic components and the bearing components are installed at each floor level (locations 1 and 2, respectively). As can be observed in the plan view, including these force-limiting connections requires introducing a gap between the GLRS and the SFRS (made through openings in the floor system) to allow relative motion between these two systems. These connections are designed to eliminate the damage expected due to the stress concentration in buildings' conventional monolithic floor-to-wall joints generated to provide kinematic compatibility between the connected structural components.

Tsampras et al.[16] performed a numerical parametric study of a 12-story example RC wall building model with force-limiting connections. They considered buckling-restrained braces or friction devices as limited-strength hysteretic components and laminated low-damping rubber bearings as bearing components. The numerical model implemented in this study considered a lumped-plasticity modeling approach for the SFRS (RC walls) and a linear-elastic modeling approach for the GLRS (RC slab-column system). The SFRS was modeled using elastic beam-column elements with reduced stiffness over the height of the wall and a nonlinear spring at the base. The GLRS was modeled using a linear-elastic moment frame with stiffness modifier factors. The force-limiting connections were modeled using an idealized elastic-plastic force-deformation response. The example building model was subjected to design-basis intensity-level ground motions to define the feasible design space of the limiting force, elastic stiffness, and post-elastic stiffness of the connections. Tsampras et al.[16] concluded that including force-limiting connections between the GLRS and the SFRS not only reduces the peak floor total acceleration, SFRS story shear, and connection force responses compared to the responses of the example building model with conventional connections but also these connections reduce the dispersion of these responses originating from the ground motion variability. They also showed that the higher-mode response contribution to the total seismic response of the building model is reduced by including force-limiting connections.

Experimental studies of full-scale force-limiting connections subjected to quasi-static seismic and dynamic sinusoidal deformation time-histories have been conducted to validate numerical models of these connections. Tsampras et al.[18] showed that the nonlinear force-deformation response of a force-limiting connection consisting of a buckling-restrained

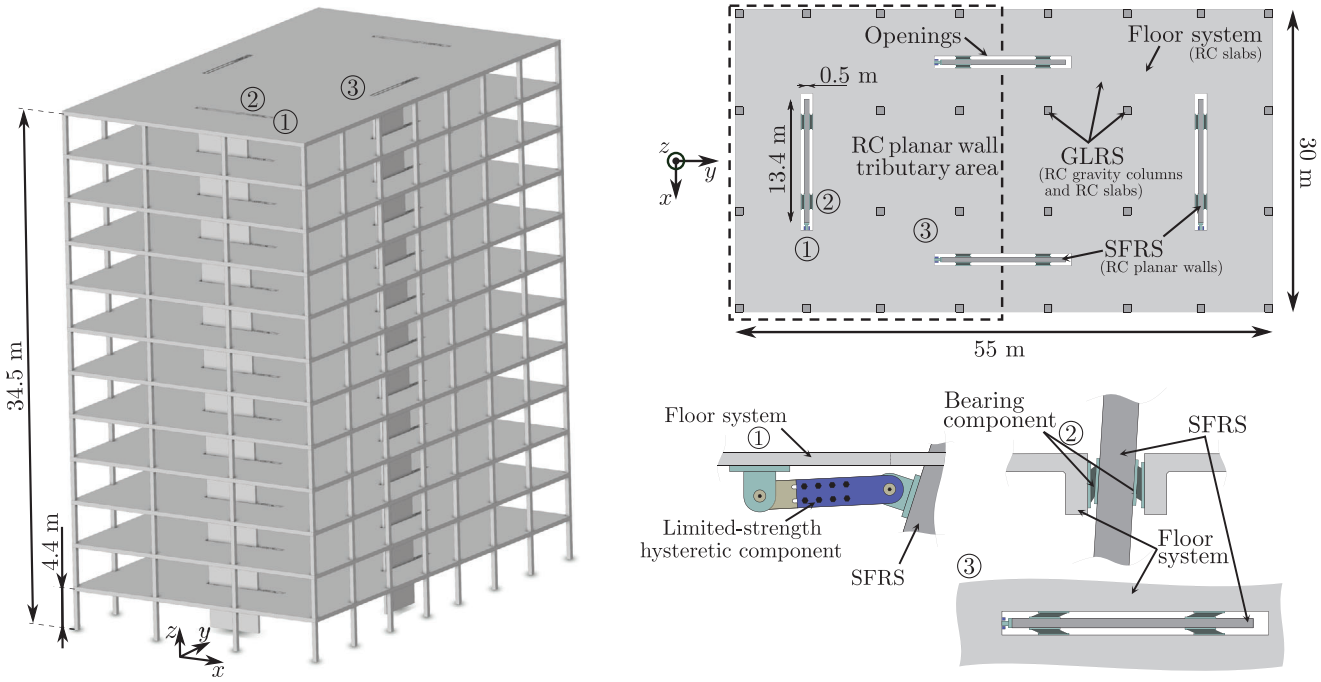

FIGURE 1 Schematic representation of the three-dimensional view, plan view, and connections between the GLRS and the SFRS of a building with force-limiting connections.

brace and rubber bearings is stable and predictable by a truss element and a set of uniaxial material models available in *OpenSees*.[24] Tsampras et al.[19] showed that the nonlinear force-deformation response of a force-limiting connection consisting of a friction device and rubber bearings can be modeled with reasonable accuracy by a bi-linear elastic-plastic model with kinematic hardening. Force-limiting connections are expected to enhance the predictability of the connection responses in buildings subjected to seismic excitation due to their higher force-deformation response modeling predictability compared to conventional connections.

Tsampras[17] showed that the modeling approach of the GLRS affects the seismic response of a 12-story building model with force-limiting connections. This study compared the results of numerical earthquake simulations of building models using reduced-stiffness linear-elastic GLRS models with different lateral stiffness. The numerical earthquake simulations showed that a reduction in the GLRS model stiffness increases GLRS story drift and connection deformation responses without significantly affecting the SFRS story shear, GLRS story shear, connection force, SFRS story drift, and floor total acceleration responses. The building model using a pin-base lean-on-column GLRS model experienced the largest connection deformation demands. The SFRS was modeled using the same lumped-plasticity modeling approach implemented by Tsampras et al.[16]; and the connections had a uniform distribution of the limiting force over the height of the building. Mayorga et al.[25] conducted a preliminary analysis that demonstrated that the modeling approach of the SFRS also influences the seismic responses of building models with force-limiting connections.

The research conducted by Tsampras et al.[16–19,22] was focused on the development, modeling, and design of force-limiting connections between the GLRS and the SFRS. These studies showed that including force-limiting connections is beneficial for the seismic performance of buildings. Nevertheless, further analyses of the numerical modeling approaches used to simulate the seismic responses of the structural components of buildings with force-limiting connections are required.

1.4 | Scope of study

This research assesses the effects of (1) the GLRS modeling approach, (2) the SFRS modeling approach, and (3) the uncertainty of the model parameters of the constitutive law of the longitudinal reinforcing steel of the SFRS on the simulated seismic responses of a 12-story RC building with force-limiting connections. This is achieved by performing nonlinear numerical simulations of two-dimensional building models subjected to far-field ground motions scaled to the

design-basis intensity-level earthquake. Building models with linear-elastic high-stiffness and unbounded (infinite) strength connections that represent buildings with conventional monolithic connections are also included in this study to compare the relative effects of the modeling approaches on buildings with and without force-limiting connections.

The GLRS of the 12-story building is composed of ordinary RC moment frames and floor slabs assumed to be made up of cast-in-place concrete. Two linear-elastic models for the GLRS are considered, a moment frame model and a lean-on-column model. The main difference between these two modeling approaches is that the lean-on-column model does not model the slabs, lumping all gravity columns in only one column. Also, the base moment reaction of the GLRS is not modeled by the lean-on-column model. The results from numerical earthquake simulations of the 12-story building models with force-limiting connections using the two GLRS modeling approaches are compared.

The SFRS of the 12-story building is composed of special RC structural planar walls with a flexural inelastic base mechanism. Two nonlinear models for the SFRS are considered, one based on the lumped-plasticity modeling approach and another one based on the distributed-plasticity modeling approach. The distributed-plasticity modeling approach can capture the distribution of the RC wall inelasticity over the height of the building whereas the lumped-plasticity modeling approach concentrates all inelastic response at the base of the walls. The RC wall models are calibrated and validated against cyclic quasi-static experimental test results available in the literature.[26–28] It is assumed that these numerical models are able to represent the expected seismic responses of the flexure-dominant inelastic base-mechanism special RC structural walls when the building models are subjected to design-basis intensity-level ground motions. The results from numerical earthquake simulations of the 12-story building models with conventional connections and force-limiting connections, respectively, using the two SFRS modeling approaches are compared.

A joint probability density function (PDF) of the model parameters of the constitutive law used to simulate the behavior of the reinforcing steel longitudinal fibers in the distributed-plasticity SFRS modeling approach is used to perform an uncertainty propagation analysis.[29,30] The uncertainty in the steel model parameters is propagated to the seismic responses of the building models with conventional connections and force-limiting connections, respectively. Monte Carlo simulation is used to generate samples in the steel model parameter space. Each steel model parameter sample defines a building model that is subjected to the same far-field ground motions scaled to the design-basis intensity-level earthquake. The distributions of the mean values of the peak structural responses of the building models are studied.

The authors acknowledge that more sophisticated modeling approaches can be considered for the simulation of the GLRS and the SFRS. However, simplified modeling approaches for the GLRS and the SFRS are acceptable for the relative comparison of different modeling approaches and the uncertainty propagation analysis of buildings with force-limiting connections subjected to design-basis intensity-level earthquakes, (1) assuming that the contribution of the inelastic response of the GLRS to the total inelastic response of the building is small compared to the contribution of the SFRS and (2) considering that force-limiting connections significantly reduce the shear demands in RC walls.

2 | TWELVE-STORY RC WALL BUILDING

The 12-story RC office building presented in Figure 1 is studied in this paper. As aforementioned, the GLRS of the building is composed of ordinary RC moment frames and floor slabs assumed to be made up of cast-in-place concrete, and the SFRS is composed of special RC structural planar walls with a flexural inelastic base mechanism. Both systems are connected through force-limiting connections. A combination of friction devices (limited-strength hysteretic component) and low-damping rubber bearings (bearing component) are used as force-limiting connections.

2.1 | Geometry and material properties

The primary building material is normal-weight concrete with $f'_c = 34.5$ MPa compressive strength reinforced with ASTM-A615 Grade 60 deformed steel bars. The height of the first story is 4.4 m and of the remaining upper stories is 2.7 m, leading to a total height of 34.5 m for the building. Each floor of this building covers a total area of 55.0 m × 30.0 m = 1650.0 m^2. The floor system is composed of 0.2-m-thick flat RC slabs which are vertically supported by 28 square RC gravity columns of 0.8 m dimension for the first six stories and 0.55 m dimension for the higher six stories. The slabs and gravity columns constitute the GLRS. Four special RC structural planar walls of 13.4 m × 0.5 m cross-sectional dimensions constitute the SFRS.

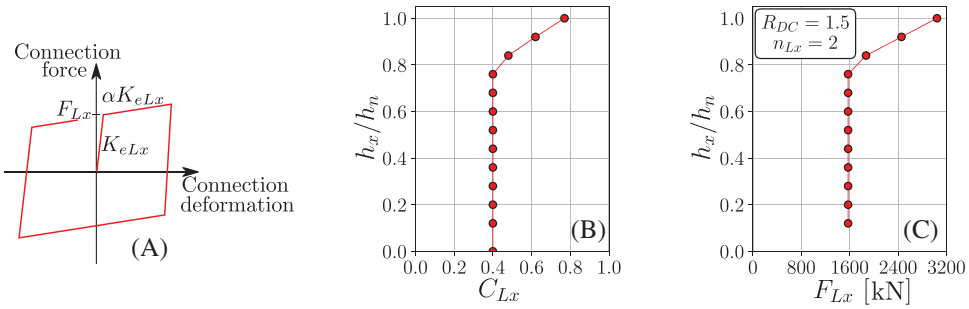

FIGURE 2 (A) Schematic representation of the force-deformation response of a force-limiting connection located at level x. (B) C_{Lx} over the height of the building. (C) F_{Lx} over the height of the building.

Each force-limiting connection consists of one friction device and four rectangular rubber bearings attached to two steel plates. Friction devices with a coefficient of friction equal to $\mu_s = 0.4$ and laminated low-damping rubber bearings are considered. The rubber bearings are made of 50 ± 5 Duro Gr 3 rubber with a shear modulus of 0.9 MPa providing a post-elastic stiffness ratio of $\alpha = 0.005$ to the force-limiting connections. These rubber bearings exhibit nearly linear-elastic behavior under large shear deformations and significant compressive stiffness that provides stable out-of-plane support to the SFRS. Design details and component dimensions of the force-limiting connections can be found in Tsampras et al.[19]

2.2 | Seismic design parameters

The building is assumed to be located in a region with high seismicity. The assumed spectral acceleration for short and 1 s periods defined in ASCE/SEI 7-22[31] are equal to $S_S = 1.50g$ and $S_1 = 0.60g$, respectively. The site class is considered as D resulting in the spectral accelerations at the maximum considered earthquake level for short and 1 s periods equal to $S_{MS} = 1.50g$ and $S_{M1} = 1.02g$, respectively. This corresponds to a seismic design category D ($S_{DS} = 1.00g$ and $S_{D1} = 0.68g$). The structural system is classified in the risk category II, and therefore, the importance factor is equal to $I_e = 1.0$. The seismic mass associated with each shear wall is 513.8 kN/g for the first floor and 782.9 kN/g for the remaining upper floors, and the seismic mass corresponding to each floor of the GLRS is 11810.0 kN/g.

2.3 | Design of GLRS and SFRS

The GLRS is designed following the requirements of the ACI-318-19 for ordinary RC frames and the SFRS is designed following the requirements of the ACI-318-19 for special RC walls.[32] The ASCE/SEI 7-22 Equivalent Lateral Force prescriptive seismic design method for conventional buildings is used to estimate the seismic demands.[31]

2.4 | Design of force-limiting deformable connections

The force at which a force-limiting connection at floor level x transitions from the linear-elastic to the post-elastic response is the design limiting force F_{Lx}, shown in Figure 2A. The values of F_{Lx} are determined by the force-based design method proposed by Tsampras and Sause.[22] This method uses a modified version of design acceleration coefficients given by the Alternative Seismic Design Forces for Floor Diaphragms per FEMA P-1050.[33] The design limiting force is computed as $F_{Lx} = (C_{Lx} w_{px})/(R_{DC} n_{Lx})$, where C_{Lx} is the design acceleration coefficient at level x, w_{px} is the seismic weight tributary to the floor diaphragm at level x, R_{DC} is the connection design force factor that accounts for the deformation capacity of the connection, and n_{Lx} is the number of force-limiting connections at level x.

Tsampras and Sause[22] concluded that F_{Lx} corresponding to a reduction factor close to $R_{DC} = 1.5$ results in acceptable seismic responses and reasonable connection deformation demands for a 12-story building with force-limiting connections. Therefore, F_{Lx} over the height of the 12-story RC wall building is computed using $R_{DC} = 1.5$, C_{Lx} over the height of the building presented in Figure 2B, $w_{px} = 11810.0$ kN, and $n_{Lx} = 2$ for $x = 1, \ldots, 12$. The resulting F_{Lx} is presented in Figure 2C.

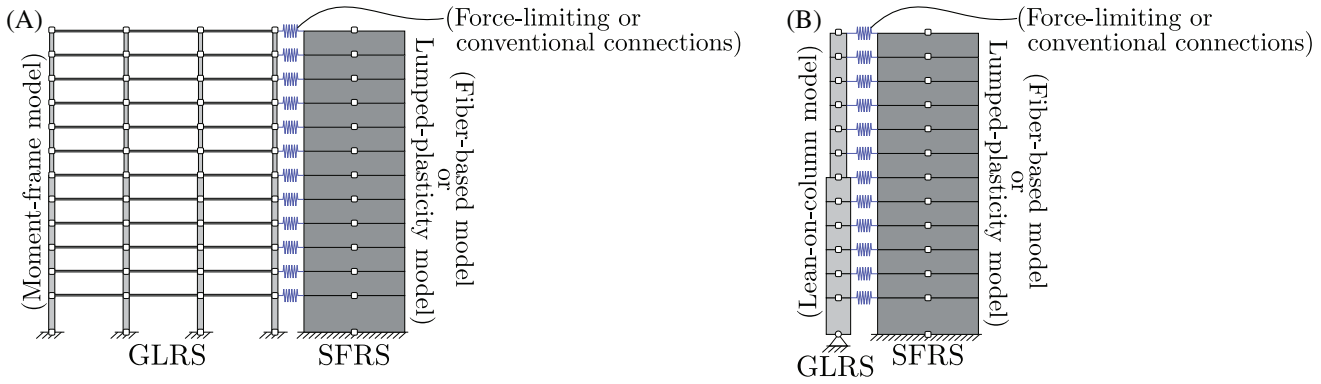

FIGURE 3 Schematic representation of the two-dimensional numerical building models implemented in this study. (A) Moment-frame GLRS model. (B) Lean-on-column GLRS model.

3 | NUMERICAL MODEL

Two-dimensional numerical models of the 12-story RC wall building considering combinations of two modeling approaches for the GLRS and two modeling approaches for the SFRS are used to assess the effects of the modeling approaches of the GLRS and the SFRS on the seismic responses of the building models with force-limiting connections. Numerical building models with conventional connections are also considered in the analysis. Figure 3 presents a schematic representation of the numerical building models implemented in this study.

3.1 | Building model assumptions

Half of the 12-story building including one RC planar wall oriented in x-direction and its tributary area (see Figure 1) is used to develop numerical models in *OpenSees*.[24] Since two-dimensional models are used, the floor diaphragm flexibility is not modeled. The moment transmitted from the slabs to the RC walls for buildings with monolithic conventional connections is neglected because it is expected that the slabs get cracked at the deformation demands induced by the design-basis intensity-level earthquakes. The conventional connections are modeled using truss elements with high axial stiffness. A 2.0% of the critical damping is assigned to modes one and three using classical damping to represent the inherent damping of the structural system. This damping percentage is assumed considering that the damping associated with the hysteretic response of the SFRS is explicitly modeled. The shear deformation of the beam-column elements is neglected considering that the aspect ratio of the RC walls is 2.6, significant nonlinear shear response is not anticipated for the intensity level of the ground motions applied to the numerical models, and the use of force-limiting connections reduces the shear demands in the RC walls preventing their excessive inelastic shear response. Geometric nonlinearity is considered by using the corotational formulation for the structural elements of the building models.

3.2 | Gravity load-resisting system modeling approaches

The GLRS is modeled through two linear-elastic modeling approaches: (1) a moment frame system (Moment-frame model) and (2) a pin-base lean-on-column system (Lean-on-column model). The Moment-frame model simulates the flat slabs using beam elements with an equivalent width of 2.5 m and considers columns with a fixed connection at the base. The Lean-on-column model does not simulate the slabs, lumping all gravity columns in only one column. Therefore, the interaction between the slabs and columns (moment-frame action) in the GLRS is not modeled. The Lean-on-column model neglects the base moment reaction of the GLRS using a pinned connection at the base of the lean-on column. The flexible Lean-on-column GLRS model is commonly used in the preliminary design of buildings to estimate an upper limit of the expected seismic-induced SFRS deformation demands. Reduction factors of 0.7 and 0.25 are applied on the cross-section moment of inertia of the columns and equivalent slab beams, respectively. These reduction factors are included to take into account the effects of the expected cracked condition and nonlinear behavior on the stiffness. The two GLRS modeling approaches can be considered as two extreme cases in terms of the lateral stiffness of the GLRS.

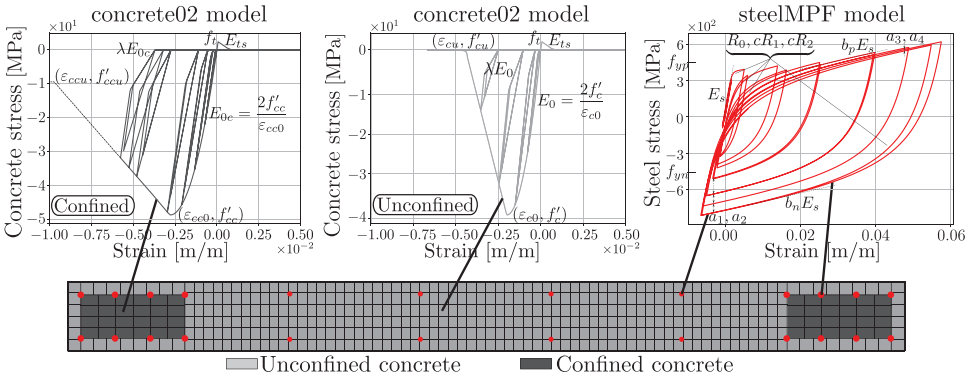

FIGURE 4 Uniaxial material constitutive laws for the unconfined concrete, confined concrete, and reinforcing steel fibers.

3.3 | Seismic force-resisting system modeling approaches

The SFRS is modeled through two nonlinear modeling approaches: (1) a distributed-plasticity modeling approach that uses *Fiber-section Force-based Beam-column*[3] elements to simulate the RC wall behavior (Fiber-based model) and (2) a lumped-plasticity modeling approach that uses reduced-stiffness linear-elastic *Euler-Bernoulli Beam-column* elements over the height of the wall with a pinned base connection and lumps the RC wall plasticity in a rotational multi-linear inelastic spring located at the base (Lumped-plasticity model). The Fiber-based model is calibrated against experimental test results available in the literature[26–28] in combination with results obtained from the sensitivity analysis of the steel model parameters conducted by Birrell et al.[30] Based on the results of the calibration of the Fiber-based model, the parameters of the Lumped-plasticity model are defined to obtain similar roof displacement versus base shear responses from both SFRS modeling approaches.

3.3.1 | Distributed-plasticity modeling approach

The *Fiber-section Force-based Beam-column* elements simulate the seismic nonlinear responses of RC walls at fiber, section, and element levels. One element per story of the 12-story building is considered. For each element, five Gauss-Lobatto integration points are used to obtain the element level response from the section level response, which is determined by the definition of the material behavior at the fiber level response. Figure 4 presents the uniaxial material constitutive laws for the unconfined concrete, confined concrete, and reinforcing steel fibers in a discretized wall cross-section. The unconfined concrete, confined concrete, and reinforcing steel fibers are shown in light gray, dark gray, and red colors, respectively. The cyclic stress-strain behavior of the unconfined and confined concrete is simulated using the *Concrete02* model[34] and the cyclic stress-strain behavior of the reinforcing steel is simulated using the *SteelMPF* model[29,35] in *OpenSees*.[24] The numerical issue of localization of the deformation in the first integration point of the element at the base of the SFRS model is addressed using the regularization method proposed by Coleman and Spacone.[36]

The parameters of the *Concrete02* model for the unconfined concrete fibers are the concrete compressive strength at 28 days f'_c, concrete strain at maximum strength ε_{c0}, concrete crushing strength f'_{cu}, concrete strain at crushing strength ε_{cu}, ratio λ between the unloading slope at ε_{cu} and initial slope $E_0 = 2f'_c/\varepsilon_{c0}$, tensile strength f_t, and tension softening stiffness E_{ts} (absolute value of the slope of the linear tension softening branch). f'_c, ε_{c0}, and ε_{cu} are obtained from the results of compressive cylinder tests of the concrete used to build the RC walls. $f'_{cu} = 0, \lambda = 0.25$, and E_{ts} equals 10% of the concrete modulus of elasticity E_c[32] are assumed. f_t is computed from the formula for the direct tensile strength given in ACI-224-01.[37]

The parameters of the *Concrete02* model for the confined concrete fibers are the concrete compressive strength at 28 days f'_{cc}, concrete strain at maximum strength ε_{cc0}, concrete crushing strength f'_{ccu}, concrete strain at crushing strength ε_{ccu}, ratio λ between the unloading slope at ε_{ccu} and initial slope $E_{0c} = 2f'_{cc}/\varepsilon_{cc0}$, f_t, and E_{ts}. f'_{cc}, ε_{cc0}, and ε_{ccu} are obtained from empirical formulas available in the literature.[32,37–39] $f'_{ccu} = 0.2f'_{cc}$ is assumed. λ, f_t, and E_{ts} are assumed equal to the same values of the parameters used for the unconfined concrete fibers.

The parameters of the *SteelMPF* model for the reinforcing steel fibers are the yielding strength in tension f_{yp}, yielding strength in compression f_{yn}, initial tangent modulus E_s, strain hardening ratio in tension b_p, strain hardening ratio in

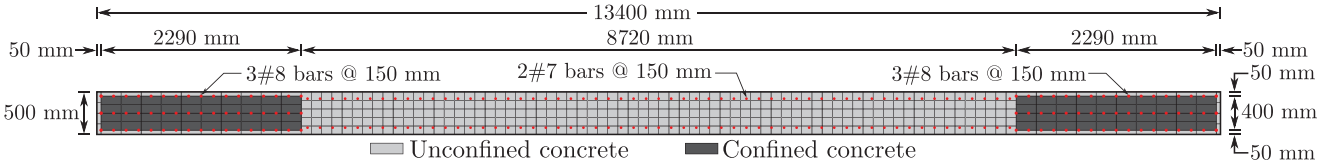

FIGURE 5 Cross-section and fiber discretization used in the Fiber-based models of the RC walls designed as the SFRS of the studied 12-story building with force-limiting connections.

compression b_n, the initial value of the curvature parameter R_0, curvature degradation parameters cR_1 and cR_2, isotropic hardening in compression parameters a_1 and a_2, and isotropic hardening in tension parameters a_3 and a_4. All these parameters except f_{yp} and f_{yn} are determined as a result of the numerical model calibration presented in the next section. f_{yp} is obtained from the material test of the reinforcing steel bars used to build the RC walls. It is assumed that $f_{yn} = f_{yp}$.

The material properties, geometry, and reinforcement details of the RC walls in the studied 12-story building are determined by following the requirements of the prescriptive seismic design method for conventional buildings.[31,32] Figure 5 shows the cross-section and fiber discretization used in the Fiber-based models of the RC walls. The unconfined concrete model parameters are assumed equal to $f'_c = -34.5$ MPa, $\varepsilon_{c0} = -0.002$ m/m, $f'_{cu} = 0.0$, $\varepsilon_{cu} = -0.004$ m/m, $\lambda = 0.25$, $f_t = 2.0$ MPa, and $E_{ts} = 0.1E_c = 2778.9$ MPa. The computed confined concrete model parameters are $f'_{cc} = -65.4$ MPa, $\varepsilon_{cc0} = -0.011$ m/m, $f'_{ccu} = -13.1$ MPa, and $\varepsilon_{ccu} = -0.069$ m/m. The yield strength is assumed equal to $f_y = 511.6$ MPa and the remaining steel model parameters are given in Table 3.

3.3.2 | Calibration of flexure-dominant inelastic base-mechanism response

This section aims to calibrate and validate the Fiber-based models that simulate the nonlinear seismic responses of the flexure-dominant inelastic base-mechanism RC walls[38] designed as the SFRS of the 12-story building with force-limiting connections. Experimental data from three documented laboratory test results of rectangular RC walls subjected to cyclic lateral quasi-static loading are utilized to calibrate and validate the Fiber-based models of the RC walls. One RC wall specimen is used for calibration and two RC wall specimens are used for validation of the numerical models. The specimens used for numerical model calibration and validation are selected from the literature taking into account the following criteria. First, structural walls with aspect ratios greater than or equal to three and different levels of confinement at the ends are considered. Second, one-quarter scale tests or larger are considered to avoid significant material size effects in the structural response. Third, specimens with material properties typically used in non-prestressed RC design are selected. The experimental base shear versus roof displacement responses of the specimens are used as target responses in the numerical model calibration and validation. The objective is not to find a numerical model that precisely replicates the nonlinear cyclic response of a specific RC wall specimen but to define numerical models that acceptably simulate the nonlinear seismic responses typically observed in flexure-dominant inelastic base-mechanism RC walls.

RC wall specimens for calibration

The specimen used for numerical model calibration is the RW2 Specimen tested by Thomsen and Wallace.[26] This specimen was tested in the context of an experimental and analytical study of RC structural walls with symmetrical and asymmetrical cross-sections designed using a displacement-based design methodology. The first specimen used for numerical model validation is the C10 Specimen tested by Elwood et al.[27] This specimen was tested to assess the effects of axial load and varied confinement detailing on the structural responses of the RC walls. In this experimental program, four large-scale rectangular RC walls were subjected to quasi-static reversed-cyclic loading for different combinations of axial load ratio, confinement depth, and inclusion/exclusion of web ties. The second specimen used for numerical model validation is the WP7 tested by Wallace et al.[28] This specimen was tested among seven one-half-scale RC walls representing the lower level of structural RC walls in 8- to 10-story buildings. In this case, the configuration and quality of boundary transverse reinforcement, the depth of the neutral axis, and the wall thickness were varied to observe their effects on the seismic performance of the walls. Table 1 lists the project, author/PI, scale, wall height, shear-span ratio, and axial load ratio corresponding to the experimental tests of the RW2, C10, and WP7 Specimens. The material properties, geometries, reinforcement details, and loading protocols of the specimens were obtained from the corresponding experimental test documentation.

TABLE 1 Project, author/PI, scale, wall height, shear-span ratio, and axial load ratio of the specimens used for numerical model calibration and validation.

Specimen	Project	Author/PI	Scale	Height h_w (mm)	Shear-span ratio $M/(VL)$	Axial load ratio $P/(A_g f'_c)$
RW2	Thomsen 1995[26]	John Thomsen and John Wallace	1/4	3657.6	3.0	0.072
C10	MBIE-1607[27]	Kenneth Elwood	1	3500.0	4.6	0.092
WP7	NEESR-1628[28]	John Wallace	1/2	2133.6	3.5	0.100

TABLE 2 Multivariate normal distribution of the parameters of the *Steel02* model[29,35] proposed by Birrell et al.[30] for the ASTM-A615 Grade 60 steel.

Parameter	Unit	Mean value μ	Coefficient of variation σ/μ (%)	Correlation matrix
f_y	MPa	512.0	5.0	$\begin{bmatrix} 1.0 & 0.3 & -0.2 & 0.2 & -0.4 & -0.9 & -0.7 \\ & 1.0 & -0.4 & 0.7 & 0.0 & -0.2 & -0.2 \\ & & 1.0 & -0.8 & -0.3 & 0.0 & 0.0 \\ & & & 1.0 & 0.3 & 0.0 & 0.0 \\ & Sym. & & & 1.0 & 0.4 & 0.4 \\ & & & & & 1.0 & 0.8 \\ & & & & & & 1.0 \end{bmatrix}$
E_s	GPa	206.0	4.0	
b	–	0.023	27.0	
cR_1	–	0.893	1.0	
cR_2	–	0.093	31.0	
a_1	–	0.035	45.0	
a_3	–	0.022	51.0	

Numerical model calibration

For each specimen, the unconfined and confined concrete model parameters are defined from the documented information of the experimental test results and empirical formulas present in the literature.[32,37–39] The steel model parameters are the outcomes of the numerical model calibration of the RW2 Specimen (except the yield strength, which was obtained from material test results of the corresponding wall specimen). The numerical model calibration uses the joint PDF of the model parameters of the *Steel02* model[29,35] proposed by Birrell et al.[30] for the ASTM-A615 Grade 60 steel. The joint PDF gives the expected values and ranges of variation of the steel model parameters. The joint PDF is a result of a sensitivity analysis of 36 cyclic tests of grade 60 reinforcing steel coupons. Birrell et al. considered R_0 as a constant and equal to 20 in the sensitivity analysis arguing that cR_1 and cR_2 are already taking into account the variability associated with the Bauschinger effect. The proposed joint PDF is a multivariate normal distribution defined by the parameters presented in Table 2. $b_p = b_n = b$ is assumed.

To define the steel model parameters, the measured base shear versus roof displacement response of the RW2 Specimen is compared with the modeled base shear versus roof displacement responses obtained from the Fiber-based models subjected to the corresponding test loading protocol.[26] The joint PDF indicates that approximately 68% of all possible values for the steel model parameters are within plus/minus one standard deviation from their corresponding mean value. A set of combinations of steel model parameters is defined perturbing each steel model parameter by plus/minus one standard deviation with respect to its mean value ($\mu \pm \sigma$) while considering the mean values of the remaining steel model parameters. Note that this is only a subset of all possible combinations of the steel model parameters.

Figure 6 shows the experimental and modeled base shear versus roof displacement responses for the RW2 Specimen using the Fiber-based model. Figure 6A corresponds to the results from the Fiber-based model using the mean values of the steel model parameters given in Table 2 (except f_y). This figure does not show a good agreement between the measured and modeled responses. It is observed that the modeled response does not simulate appropriately the state of stiffness and curvature of the response in the reversal branches. Additionally, a smaller maximum base shear response is predicted by the numerical model at positive roof displacement responses compared to the experimental test results.

Figure 6B shows the effects of the variation of plus/minus one standard deviation of E_s, b, cR_1, cR_2, a_1, and a_3 on the modeled base shear versus roof displacement response. The coefficients of variation of E_s and cR_1 are 4.0% and 1.0%, respectively, which are small compared to the coefficients of variation of the other steel model parameters. As a result, the modeled responses appear to be less sensitive to the one standard deviation variations of E_s and cR_1, respectively. However, it was checked that further variations of E_s and cR_1 primarily affect the flexural stiffness and the transition from the elastic to the post-elastic behavior of the modeled response. An increase of b produces a small increase in the post-elastic stiffness

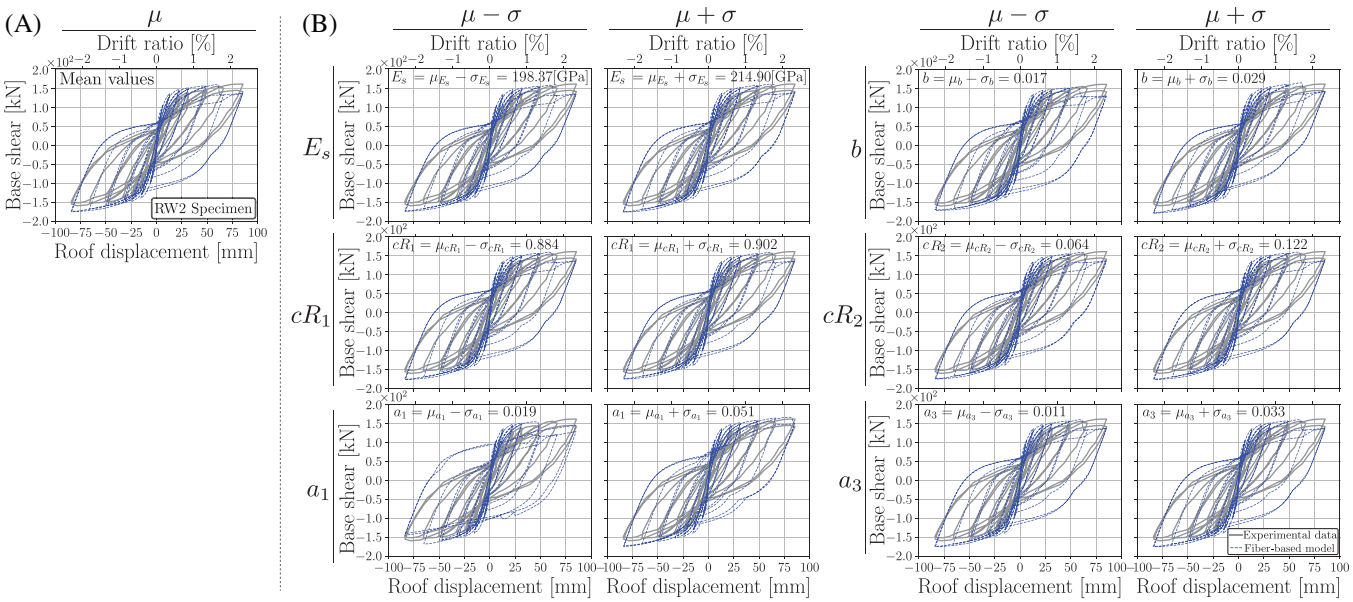

FIGURE 6 Experimental and modeled base shear versus roof displacement responses. (A) Mean values and (b) mean values plus/minus one standard deviation variations of E_s, b, cR_1, cR_2, a_1, and a_3. RW2 Specimen.

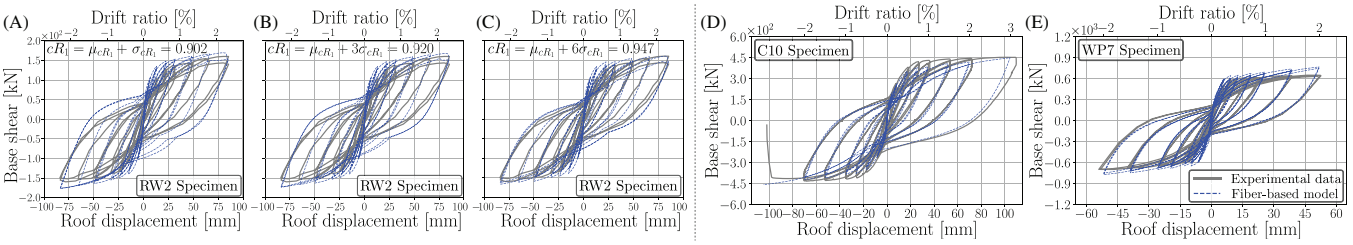

FIGURE 7 Experimental and modeled base shear versus roof displacement responses. Numerical models using $E_s = \mu_{E_s} = 206.0$ GPa, $b = \mu_b + \sigma_b = 0.029$, $cR_2 = \mu_{cR_2} = 0.093$, $a_1 = \mu_{a_1} + \sigma_{a_1} = 0.051$, $a_3 = \mu_{a_3} = 0.022$, and (A) $cR_1 = \mu_{cR_1} + \sigma_{cR_1}$, (B) $cR_1 = \mu_{cR_1} + 3\sigma_{cR_1}$, and (C) $cR_1 = \mu_{cR_1} + 6\sigma_{cR_1}$ for the RW2 Specimen. Numerical models using the steel model parameters given in Table 3 for (D) the C10 Specimen and (E) the WP7 Specimen.

of the modeled response resulting in a better agreement between the post-elastic stiffness of the measured and modeled responses when $b = \mu_b + \sigma_b = 0.029$. There are no appreciable effects of cR_2 and a_3 on the modeled responses for the considered parameter ranges of variation. The maximum strain response in compression is limited by the concrete strain response in compression. Therefore, the increase of the difference between the maximum strain responses in compression and tension used to estimate the isotropic hardening in tension (shift of the yield asymptotes of the stress responses in tension[30]) is limited. As a result, the effect of the isotropic hardening associated with a_3 on the modeled responses is limited. An increase of a_1 makes the hysteretic response less wide and increases the maximum base shear responses at large deformations. The modeled response approximates reasonably well the measured maximum base shear responses at positive roof displacement responses when $a_1 = \mu_{a_1} + \sigma_{a_1} = 0.051$.

The base shear versus roof displacement response from the experimental test and the base shear versus roof displacement response from the numerical model using $E_s = \mu_{E_s} = 206.0$ GPa, $b = \mu_b + \sigma_b = 0.029$, $cR_1 = \mu_{cR_1} + \sigma_{cR_1} = 0.902$, $cR_2 = \mu_{cR_2} = 0.093$, $a_1 = \mu_{a_1} + \sigma_{a_1} = 0.051$, and $a_3 = \mu_{a_3} = 0.022$ are compared in Figure 7A. This set of steel model parameters combines the effects of simultaneously adding one standard deviation to the mean values of b, cR_1, and a_1 while considering the mean values of the remaining steel model parameters. The modeled response has a better agreement with the experimental response compared to the modeled response using the mean values of the steel model parameters. The numerical model reaches the maximum base shear response at the largest positive roof displacement response; however, the stiffness and curvature of the response in the reversal branches are larger than in the case of the experimental response. To reduce the curvature of the response in the reversal branches, the parameter cR_1 is further increased.

TABLE 3 Steel model parameters used to simulate the seismic responses of the flexure-dominant inelastic base-mechanism RC walls designed as the SFRS of the 12-story building with force-limiting connections.

Parameter	Unit	Mathematical expression	Numerical value
E_s	GPa	μ_{E_s}	206.0
b	–	$\mu_b + \sigma_b$	0.029
cR_1	–	$\mu_{cR_1} + 6\sigma_{cR_1}$	0.947
cR_2	–	μ_{cR_2}	0.093
a_1	–	$\mu_{a_1} + \sigma_{a_1}$	0.051
a_3	–	μ_{a_3}	0.022

Figures 7B and 7C present the modeled response using $cR_1 = \mu_{cR_1} + 3\sigma_{cR_1} = 0.920$ and $cR_1 = \mu_{cR_1} + 6\sigma_{cR_1} = 0.947$, respectively. These figures show that the experimental and the modeled base shear versus roof displacement responses result in a similar evolution of stiffness when $cR_1 = \mu_{cR_1} + 6\sigma_{cR_1} = 0.947$. Thus, the steel model parameters given in Table 3 are considered candidates to simulate the seismic responses of the flexure-dominant inelastic base-mechanism RC walls designed as the SFRS of the 12-story building with force-limiting connections.

The C10 and WP7 Specimens are used to validate the Fiber-based models using the steel model parameters given in Table 3. It is verified whether the numerical model used to simulate the base shear versus roof displacement response of the RW2 Specimen can reasonably capture the base shear versus roof displacement responses of the C10 and WP7 Specimens, both expected to have cyclic nonlinear behavior similar to the cyclic nonlinear behavior of the RW2 Specimen. Figures 7D and 7E show the experimental and modeled base shear versus roof displacement responses for the C10 and WP7 Specimens, respectively. It is observed that the numerical models using the steel model parameters given in Table 3 can simulate the experimental test responses of these two specimens reasonably well. For the C10 Specimen, the numerical model can capture the loading and unloading stiffness and the curvature of the response; however, this model underestimates the maximum base shear responses at the end of each cycle. In the case of the WP7 Specimen, the numerical model can capture the initial and reversal stiffness and the curvature of the response; however, this model overestimates the post-elastic stiffness making the maximum base shear response at the end of each cycle larger than the one observed in the experimental test response. Overall, it can be expected that the Fiber-based models using the steel model parameters given in Table 3 simulate reasonably well the seismic responses of the flexure-dominant inelastic base-mechanism RC walls. So, these steel model parameters define the calibrated Force-based models used to simulate the seismic responses of the RC walls designed as the SFRS of the 12-story building with force-limiting connections.

3.3.3 | Lumped-plasticity modeling approach

The Lumped-plasticity model considers a reduction factor of 0.35 applied on the gross cross-sectional moment of inertia of the linear-elastic *Euler-Bernoulli Beam-column* elements that model the RC wall over the height of the building. This reduction factor is applied to represent the stiffness reduction because of cracking and nonlinear behavior. The flexural inelastic base mechanism is simulated using a zero-length rotational spring with a macroscopic inelastic moment-rotation response defined using the *Pinching4*[40] material model in *OpenSees*.[24] The parameters of the *Pinching4* material model are set to obtain a base shear versus roof displacement response similar to the base shear versus roof displacement response obtained by implementing the Fiber-based model using the steel model parameters given in Table 3. The base shear versus roof displacement responses from the Fiber-based and Lumped-plasticity models are presented in Figure 8. The base shear versus roof displacement response using the resulting parameters of the *Pinching4* material model matches reasonably well the base shear versus roof displacement response computed using the Fiber-based model. The Lumped-plasticity model captures the initial tangent stiffness in the loading and unloading branches of the response using the Fiber-based model; however, the post-elastic stiffness before a reversal roof displacement is lower when the Lumped-plasticity model is used. The reason for this is that the Lumped-plasticity model does not simulate the isotropic hardening of the stress-strain behavior of the longitudinal reinforcing steel. The resulting parameters of the *Pinching4* material model are: $ePf_1 = eNf_1 = 3.082 \times 10^5$ kNm, $ePf_2 = eNf_2 = 4.887 \times 10^5$ kNm, $ePf_3 = eNf_3 = 5.910 \times 10^5$ kNm, $ePf_4 = eNf_4 = 5.342 \times 10^5$ kNm, $ePd_1 = eNd_1 = 8.90 \times 10^{-4}$ rad, $ePd_2 = eNd_2 = 2.31 \times 10^{-2}$ rad, $ePd_3 = eNd_3 = 4.39 \times 10^{-2}$ rad, $ePd_4 = eNd_4 = 5.25 \times 10^{-2}$ rad, $rDispP = rDispN = rForceP = rForceN = 0.85$,

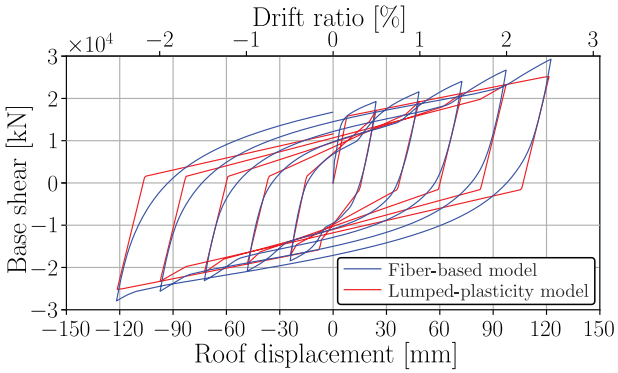

FIGURE 8 Base shear versus roof displacement response. Fiber-based and Lumped-plasticity SFRS models.

$uForceP = uForceN = 0.05$, $gK_1 = 0.25$, $gK_2 = gK_3 = gK_4 = 0.0$, $gK_{\text{Lim}} = 0.995$, $gD_1 = gD_2 = gD_3 = gD_4 = gD_{\text{Lim}} = 0.0$, $gF_1 = gF_2 = gF_3 = gF_4 = gF_{\text{Lim}} = 0.0$, $gE = 10.0$, and $dmg_{\text{Type}} =$ "cycle".

3.4 | Force-limiting deformable connection modeling approach

As recommended in Tsampras et al.,[16] an elastic perfectly-plastic model is used to simulate the force-deformation response of the friction devices and a linear-elastic model is used to simulate the force-deformation response of the rubber bearings. To combine these two force-deformation responses, the force-limiting connections are modeled using the *Corotational Truss* elements with *Steel01* material in *OpenSees*.[24]

4 | SEISMIC EXCITATION

The 12-story building models are subjected to 18 ground motions selected from the 44 FEMA P-695 far-field ground motion data set.[41] The recorded ground motions are scaled so that the average spectral response accelerations of the 18 scaled ground motions match the spectral response accelerations of the ASCE/SEI 7-22[31] design basis response spectrum over the range of periods between 0.6 and 2.0 s.[31,42] For computing the spectral response accelerations, a 5% of the critical damping is considered. The list of the selected ground motions including the corresponding scale factors, the design acceleration response spectrum, the acceleration response spectrum of the 18 scaled ground motions, and the average acceleration response spectrum can be found in Tsampras et al.[22]

5 | NUMERICAL SIMULATION RESULTS

Numerical earthquake simulations are conducted to assess the effects of the modeling approaches of the SFRS and the GLRS on the seismic responses of the 12-story RC wall building models subjected to the 18 design-basis intensity-level ground motions. Section 5.1 assesses the effect of the GLRS modeling approach by comparing the peak seismic responses obtained from building models using the Moment-frame and Lean-on-column GLRS models introduced in Section 3.2. The building model with force-limiting connections using the Fiber-based model for the SFRS is considered in this analysis. Section 5.2 assesses the effect of the SFRS modeling approach by comparing the peak seismic responses obtained from building models using the Fiber-based and Lumped plasticity SFRS models introduced in Sections 3.3.1 and 3.3.3, respectively. The building models with conventional connections and force-limiting connections, respectively, using the Lean-on-column model for the GLRS are considered in this analysis. Section 5.3 assesses the effects of the uncertainty in the model parameters of the constitutive law of the longitudinal reinforcing steel of the SFRS on the variability of the seismic responses of the building models through Monte Carlo earthquake simulation. The building models with conventional connections and force-limiting connections, respectively, using the Lean-on-column GLRS model and the Fiber-based SFRS model are considered in this analysis. Histograms of the mean values of the peak seismic responses of the building models with conventional connections and force-limiting connections, respectively, are compared. Table 4 summarizes the numerical models compared in the following sections.

TABLE 4 Numerical models compared in Sections 5.1, 5.2, and 5.3.

Section	GLRS model	SFRS model	GLRS-to-SFRS connection
5.1	Moment-frame	Fiber-based	Force-limiting
5.1, 5.2, 5.3	Lean-on-column	Fiber-based	Force-limiting
5.2	Lean-on-column	Lumped-plasticity	Conventional
5.2	Lean-on-column	Lumped-plasticity	Force-limiting
5.2, 5.3	Lean-on-column	Fiber-based	Conventional

TABLE 5 Mean values and standard deviations (in parenthesis) and the corresponding percentage (%) of variation due to the change in the GLRS modeling approach of the peak SFRS base shear, SFRS base moment, roof total acceleration, SFRS 12th-story drift, SFRS confined concrete minimum strain at the base, SFRS reinforcing steel maximum strain amplitude at the base, roof connection force, 3rd-floor connection deformation, GLRS 12th-story shear, and GLRS 12th-story drift responses. Twelve-story building models with force-limiting connections using the Moment-frame and Lean-on-column GLRS models, and the Fiber-based SFRS model.

		Mean value (Standard deviation)		
Response	Unit	Moment-frame GLRS model	Lean-on-column GLRS model	% of variation
Peak SFRS base shear	kN	17035.9 (1166.7)	16525.3 (976.3)	−3.0% (−16.3%)
Peak SFRS base moment	kNm	320488.7 (25007.6)	322081.7 (30675.8)	+0.5% (+22.7%)
Peak roof total acceleration	g	0.659 (0.061)	0.542 (0.016)	−17.8% (−73.8%)
Peak SFRS 12th-story drift	rad	0.0104 (0.0020)	0.0115 (0.0033)	+10.6% (+65.0%)
Peak SFRS confined concrete minimum strain at the base	m/m	0.00369 (0.00109)	0.00399 (0.00155)	+8.1% (+42.2%)
Peak SFRS reinf. steel max. strain amplitude at the base	m/m	0.0244 (0.0077)	0.0231 (0.0104)	−5.3% (+35.1%)
Peak roof connection force	kN	2987.1 (146.0)	3099.7 (46.0)	+3.8% (−68.5%)
Peak 3rd-floor connection deformation	mm	22.94 (13.76)	21.33 (14.12)	−7.0% (+2.6%)
Peak GLRS 12th-story shear	kN	1706.3 (305.5)	258.0 (83.4)	−84.9% (−72.7%)
Peak GLRS 12th-story drift	rad	0.0100 (0.0019)	0.0116 (0.0029)	+16.0% (+52.6%)

5.1 | Effect of the GLRS modeling approach

The effects of the GLRS modeling approach on the peak SFRS story shear, SFRS moment, floor total acceleration, SFRS story drift, SFRS confined concrete minimum strain, SFRS reinforcing steel maximum strain amplitude, connection force, connection deformation, GLRS story shear, and GLRS story drift responses are assessed for the 12-story building models with force-limiting connections. The results of the numerical earthquake simulations considering the 18 design-basis intensity-level ground motions are presented in Figure 9. Each circular marker represents the peak response generated by one ground motion and each square marker represents the mean value of the peak responses from all ground motions at the floor or story indicated in the horizontal axis. The gray markers correspond to the peak seismic responses of the building model using the Moment-frame GLRS model and the orange markers correspond to the peak seismic responses of the building model using the Lean-on-column GLRS model. Table 5 lists the mean values and standard deviations (in parenthesis) of the peak SFRS base shear, SFRS base moment, roof total acceleration, SFRS 12th-story drift, SFRS confined concrete minimum strain at the base, SFRS reinforcing steel maximum strain amplitude at the base, roof connection force, 3rd-floor connection deformation, GLRS 12th-story shear, and GLRS 12th-story drift responses. The table also includes the percentage of variation (% of variation) of the mean values and standard deviations (in parenthesis) of the peak responses due to the change in the GLRS modeling approach. The percentage of variation is computed as the relative difference between the peak responses obtained using the Moment-frame and Lean-on-column GLRS models, respectively, as a percentage of the corresponding peak response obtained using the Moment-frame GLRS model.

Figures 9A, 9B, 9C, 9E, 9F, 9G, and Table 5 show that the mean values and the corresponding dispersion of the peak SFRS story shear, peak SFRS moment, floor total acceleration, SFRS confined concrete minimum strain, SFRS reinforcing steel maximum strain amplitude, and connection force responses of the 12-story building models with force-limiting

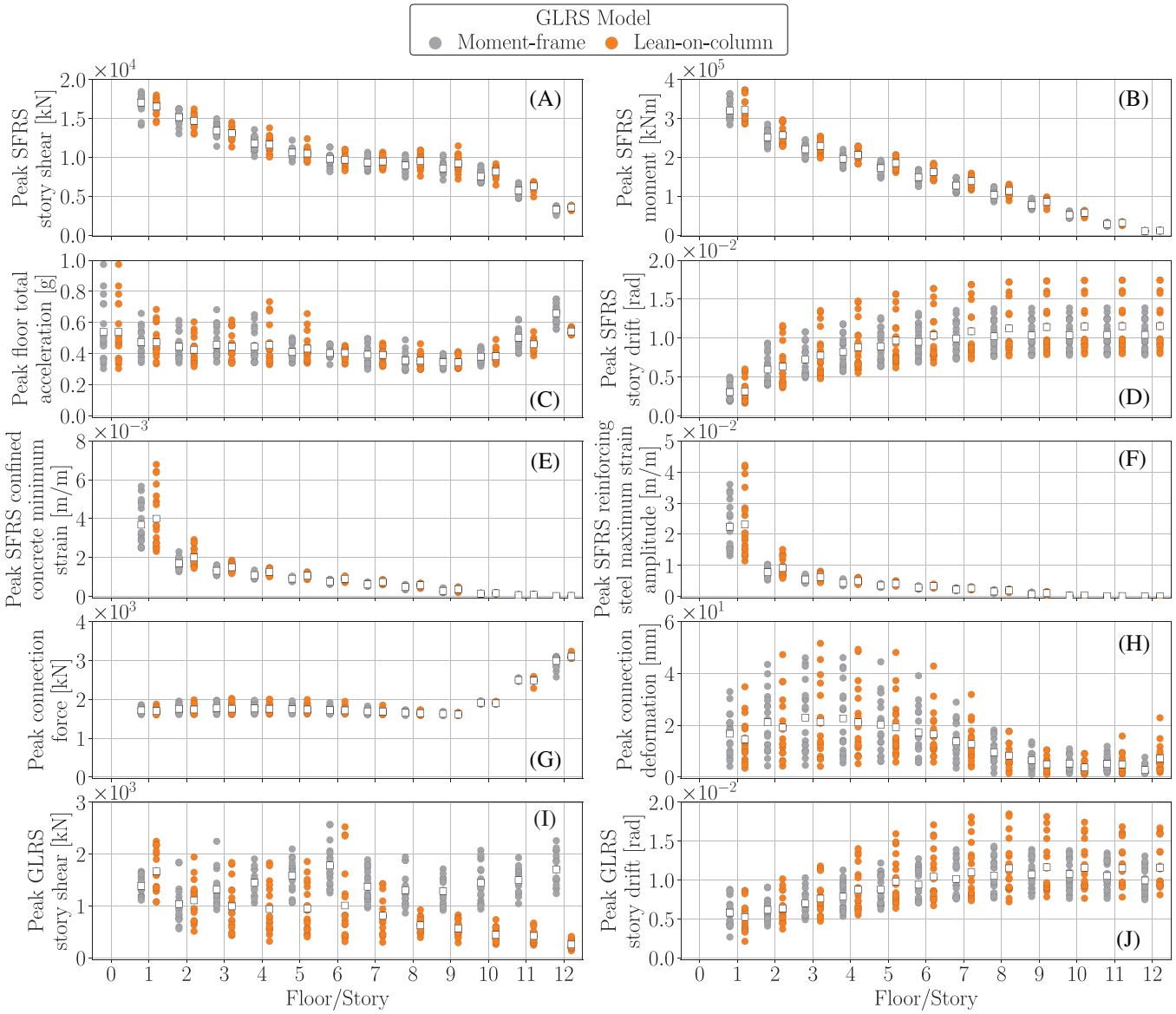

FIGURE 9 Peak (A) SFRS story shear, (B) SFRS moment, (C) floor total acceleration, (D) SFRS story drift, (E) SFRS confined concrete minimum strain, (F) SFRS reinforcing steel maximum strain amplitude, (G) connection force, (H) connection deformation, (I) GLRS story shear, and (J) GLRS story drift responses from the 18 design-basis intensity-level ground motions, and the corresponding mean values (white square markers). Twelve-story building models with force-limiting connections using the Moment-frame and Lean-on-column GLRS models, and the Fiber-based SFRS model.

connections are not practically affected by the change in the GLRS modeling approach. However, the standard deviations of the peak roof total acceleration and roof connection force responses are reduced by 73.8% and 68.5%, respectively, when the Lean-on-column GLRS model replaces the Moment-frame GLRS model.

Figures 9D, 9J, and Table 5 indicate that the mean values and the corresponding dispersion of the peak SFRS story drift and GLRS story drift responses of the building models with force-limiting connections are moderately affected by the change in the GLRS modeling approach. These results are expected because the Lean-on-column GLRS model does not simulate the base moment reaction and the moment-frame action of the GLRS. The reduced lateral stiffness of the Lean-on-column GLRS model increases the story drift responses.

Figure 9H and Table 5 show that the mean values and the corresponding dispersion of the peak connection deformation responses of the building models with force-limiting connections are not practically affected by the change in the GLRS modeling approach. Noticeable differences in the peak connection deformation responses are observed at the roof level, but the mean values of the peak connection deformation responses at that level are lower than 8.0 mm with a lower

peak response dispersion compared with those at the mid-height of the building. Tsampras[17] showed that the differences between the connection deformation responses due to a change in the GLRS modeling approach can be mainly observed at higher floors. However, Tsampras considered a Lumped-plasticity modeling approach for the SFRS and a uniform distribution of F_{Lx} over the height of the building models used to conduct numerical earthquake simulations. This suggests that the effect of the GLRS modeling approach is reduced by considering the nonuniform distribution of F_{Lx} given by the design method proposed by Tsampras and Sause.[22]

Figure 9I and Table 5 indicate that the mean values of the peak GLRS story shear responses of the building model with force-limiting connections at the higher stories are significantly lower when the Lean-on-column GLRS model is considered. However, the differences in the GLRS story shear responses due to the change in the GLRS modeling approach do not affect the SFRS story shear responses, which are an order of magnitude larger than the GLRS story shear responses.

The results of the numerical earthquake simulations indicate that the relative effects of the two studied GLRS modeling approaches on the seismic responses of the 12-story building models with force-limiting connections are limited in the context of performance-based seismic design and assessment.

5.2 | Effect of the SFRS modeling approach

The effects of the SFRS modeling approach on the peak SFRS story shear, SFRS moment, floor total acceleration, SFRS story drift, SFRS confined concrete minimum strain, SFRS reinforcing steel maximum strain amplitude, connection force, and connection deformation responses are assessed for the 12-story building models with conventional connections and force-limiting connections, respectively. The results of the numerical earthquake simulations are presented in Figure 10 following the same format used to present the results in Figure 9. The blue markers correspond to the building model with conventional connections using the Fiber-based SFRS model, red markers correspond to the building model with conventional connections using the Lumped-plasticity SFRS model, orange markers correspond to the building model with force-limiting connections using the Fiber-based SFRS model, and green markers correspond to the building model with force-limiting connections using the Lumped-plasticity SFRS model. Table 6 lists the mean values and standard deviations (in parenthesis) of the peak SFRS base shear, SFRS base moment, roof total acceleration, SFRS 12th-story drift, SFRS confined concrete minimum strain at the base, SFRS reinforcing steel maximum strain amplitude at the base, roof connection force, and 3rd-floor connection deformation responses. The table also includes the percentage of variation (% of variation) of the mean values and standard deviations (in parenthesis) of the peak responses due to the change in the SFRS modeling approach. The percentage of variation is computed as the relative difference between the peak responses obtained using the Fiber-based and Lumped-plasticity SFRS models, respectively, as a percentage of the corresponding peak response obtained using the Fiber-based SFRS model.

The GLRS story shear and GLRS story drift responses are not considered in this section. The peak GLRS story shear responses are significantly affected by the change in the GLRS modeling approach, and they are one order of magnitude lower than the peak SFRS story shear responses (see Section 5.1). The peak GLRS story drift responses are similarly affected by the change in the SFRS modeling approach compared with the peak SFRS story drift responses already included in this section.

Figures 10A, 10C, and 10G show that the mean values and the corresponding dispersion of the peak SFRS story shear, floor total acceleration, and connection force responses of the 12-story building models with conventional connections are noticeably affected by the change in the SFRS modeling approach, whereas these peak responses for the building models with force-limiting connections are considerably less affected by the change in the SFRS modeling approach. Table 6 shows that the magnitudes of the percentages of variation in the mean values of the peak SFRS base shear, roof total acceleration, and roof connection force responses due to the change in the SFRS modeling approach considerably drop from 21.8%, 46.9%, and 50.9% for the building models with conventional connections to 4.0%, 2.2%, and 1.9% for the building models with force-limiting connections, respectively. The magnitudes of the percentages of variation in standard deviations drop from 44.4%, 39.8%, and 42.4% for the building models with conventional connections to 20.9%, 18.8%, and 33.9% for the building models with force-limiting connections, respectively. However, the standard deviations of the peak responses of the building models with force-limiting connections are one to two orders of magnitude smaller than those for the building models with conventional connections.

Table 6 indicates that the mean values of the peak SFRS base moment responses of the building models with conventional connections and force-limiting connections, respectively, are not practically affected and the corresponding standard deviations are moderately affected by the change in the SFRS modeling approach. This is expected because

TABLE 6 Mean values and standard deviations (in parenthesis) and the corresponding percentage (%) of variation due to the change in the SFRS modeling approach of the peak SFRS base shear, SFRS base moment, roof total acceleration, SFRS 12th-story drift, SFRS confined concrete minimum strain at the base, SFRS reinforcing steel maximum strain amplitude at the base, roof connection force, and 3rd-floor connection deformation responses. Twelve-story building models with conventional connections and force-limiting connections, respectively, using the Lean-on-column GLRS model, and the Fiber-based and Lumped-plasticity SFRS models.

		Mean value (Standard deviation)					
		Conventional connections			Force-limiting connections		
Response	**Unit**	**Fiber-based**	**Lumped-plasticity**	**% of variation**	**Fiber-based**	**Lumped-plasticity**	**% of variation**
Peak SFRS base shear	kN	26419.4 (7728.1)	32167.1 (11162.4)	+21.8% (+44.4%)	16525.3 (976.3)	17185.5 (772.5)	+4.0% (−20.9%)
Peak SFRS base moment	kNm	334893.0 (29017.3)	346645.4 (16834.9)	+3.5% (−42.0%)	322081.7 (30675.8)	342409.7 (18010.9)	+6.3% (−41.3%)
Peak roof total acceleration	g	1.014 (0.415)	1.490 (0.580)	+46.9% (+39.8%)	0.542 (0.016)	0.554 (0.019)	+2.2% (+18.8%)
Peak SFRS 12th-story drift	rad	0.0116 (0.0027)	0.0119 (0.0024)	+2.6% (−11.1%)	0.0115 (0.0033)	0.0108 (0.0024)	−6.1% (−27.3%)
Peak SFRS confined concrete min. strain at the base	m/m	0.00471 (0.00141)	– (–)	– (–)	0.00399 (0.00155)	– (–)	– (–)
Peak SFRS reinf. steel max. strain amplitude at the base	m/m	0.0281 (0.0094)	– (–)	– (–)	0.0231 (0.0104)	– (–)	– (–)
Peak roof connection force	kN	5835.8 (2397.2)	8806.1 (3413.4)	+50.9% (+42.4%)	3099.7 (46.0)	3159.4 (61.6)	+1.9% (+33.9%)
Peak 3rd-floor connection deformation	mm	0.00 (–)	0.00 (–)	– (–)	21.33 (14.12)	21.04 (12.63)	−1.4% (−10.6%)

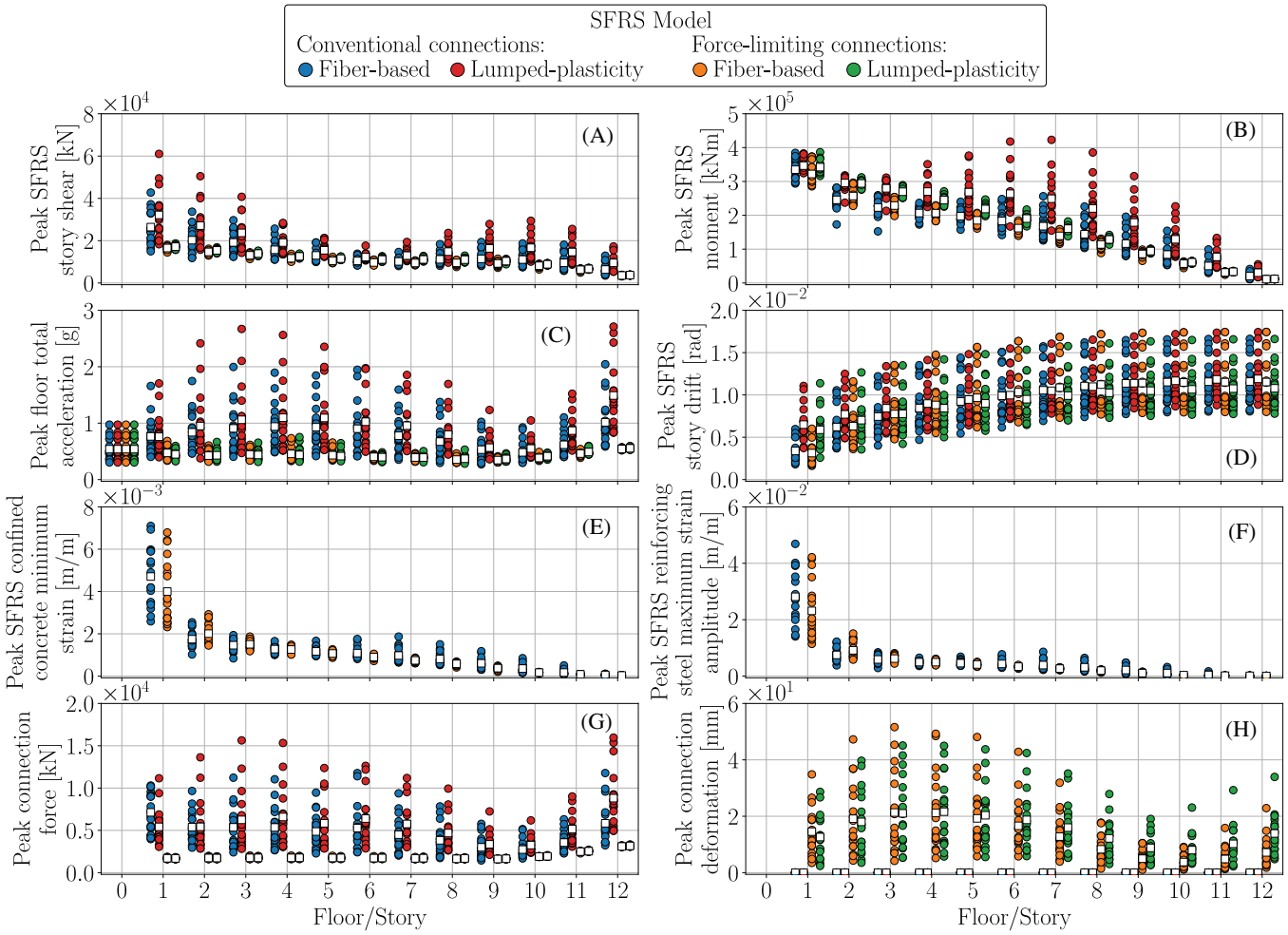

FIGURE 10 Peak (A) SFRS story shear, (B) SFRS moment, (C) floor total acceleration, (D) SFRS story drift, (E) SFRS confined concrete minimum strain, (F) SFRS reinforcing steel maximum strain amplitude, (G) connection force, and (H) connection deformation responses from the 18 design-basis intensity-level ground motions, and the corresponding mean values (white square markers). Twelve-story building models with conventional connections and force-limiting connections, respectively, using the Lean-on-column GLRS model, and the Fiber-based and Lumped-plasticity SFRS models.

the SFRS is designed to develop a flexural inelastic mechanism at the base that limits the SFRS base moment response. However, Figure 10B shows that the SFRS moment responses over the height of the building models with conventional connections are considerably affected by the change in the SFRS modeling approach. The maximum peak SFRS moment response of the building model with conventional connections using the Lumped-plasticity SFRS model occurs at the 7th story. This maximum peak value is obtained when the building model is subjected to the scaled CLW-LN component of the Landers (1992) seismic event. The time-history of the SFRS 7th-story moment response of the building model with conventional connections using the Lumped-plasticity SFRS model induced by the scaled CLW-LN component is presented in Figure 11A. The spectrogram of the SFRS 7th-story moment response shown in Figure 11B indicates that the predominant frequency content at the instant when the peak SFRS 7th-story moment response occurs is $f = 3.809$ Hz. This frequency is approximately equal to the second-mode frequency ($f_2 = 3.817$ Hz) computed considering the initial state of the stiffness of the building model with conventional connections using the Lumped-plasticity SFRS model. In addition, the acceleration response spectrum of the scaled CLW-LN component is shown in Figure 12A. The solid and dashed lines in this figure represent the second-mode period computed at the beginning of the earthquake simulations ($t = 0$ s) and at the time instant when the peak SFRS 7th-story moment response occurs, respectively. It is noted that the spectral response acceleration computed at the overlapped second-mode periods of the building model with conventional connections using the Lumped-plasticity SFRS model coincides with the peak value of the acceleration response spectrum. Therefore, it can be concluded that the maximum peak SFRS story moment response occurs at the mid-height of the building model with

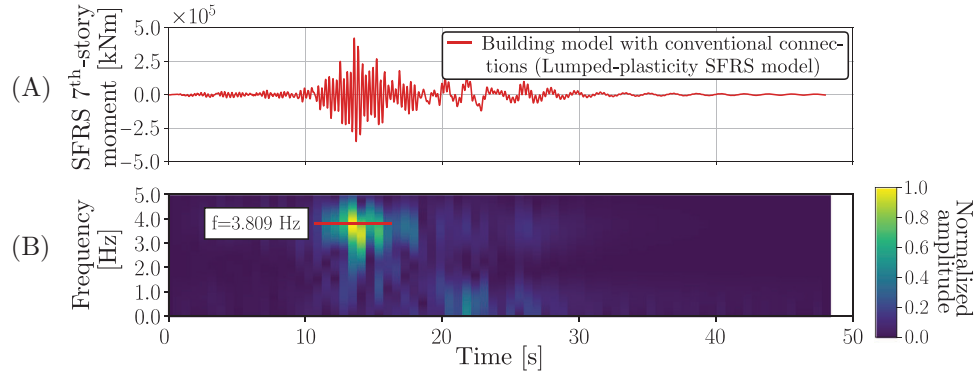

FIGURE 11 (A) Time-history of the SFRS 7th-story moment response induced by the scaled CLW-LN component of the Landers (1992) seismic event and (B) its spectrogram. Twelve-story building model with conventional connections using the Lean-on-column GLRS model and the Lumped-plasticity SFRS model.

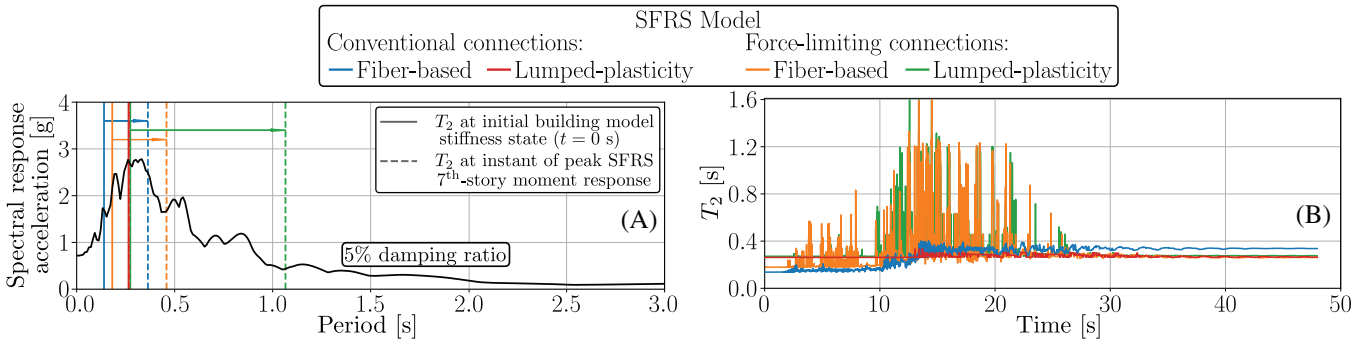

FIGURE 12 (A) Acceleration response spectrum of the scaled CLW-LN component of the Landers (1992) seismic event and (B) the evolution of the second-mode period (T_2) over time during the scaled CLW-LN component of the Landers (1992) seismic event. Twelve-story building models with conventional connections and force-limiting connections, respectively, using the Lean-on-columns GLRS model, and the Fiber-based and Lumped-plasticity SFRS models.

conventional connections using the Lumped-plasticity SFRS model due to the significant contribution of the second-mode response to the total seismic response of the building model.

Figure 10B shows that the peak SFRS moment responses and the corresponding dispersion at the mid-height of the building model with conventional connections using the Fiber-based SFRS model are smaller compared to these peak responses for the building model with conventional connections using the Lumped-plasticity SFRS model. The use of the Fiber-based SFRS model for the simulation of the flexural response of the RC wall allows for the simulation of the evolution of concrete cracking over the height of the wall. The cracking of the wall modifies the state of the stiffness and, as a result, modifies the seismic response of the building model. The modification of the seismic response results in reduced SFRS moment responses at the mid-height of the building model using the Fiber-based SFRS model. The peak SFRS moment responses and the corresponding dispersion at the mid-height of the building model with force-limiting connections using the Fiber-based SFRS model are smaller compared to these peak responses for the building model with conventional connections using the Fiber-based SFRS model. Thus, the use of force-limiting connections instead of conventional connections allows for further modification of the seismic responses of the building models with significant effects on the dispersion of the SFRS moment responses. As a result, the peak SFRS moment responses at the mid-height of the building models with force-limiting connections are less sensitive to the change in the SFRS modeling approach compared to these peak responses for the building models with conventional connections.

Figure 12B shows the evolution of the second-mode period (T_2) over time of the building models with conventional connections and force-limiting connections, respectively, obtained from the numerical earthquake simulations using the scaled CLW-LN component of the Landers (1992) seismic event as the ground motion excitation. The numerical results for the building models using both SFRS modeling approaches are presented. The second-mode period at each time step is obtained using the mass matrix (constant) and the instantaneous tangent stiffness matrix computed at the corresponding

time step. The Fiber-based SFRS models assume that the concrete in the RC walls is uncracked at the beginning of the ground motion. The Lumped-plasticity SFRS models consider stiffness reduction factors to account for cracking and nonlinear behavior of the RC walls over the height of the building. As a result, the building models using the Lumped-plasticity SFRS model are more flexible at $t = 0$ s compared to the building models using the Fiber-based SFRS model; therefore, the initial second-mode periods of the building models using the Lumped-plasticity SFRS models are longer. The initial stiffness of the force-limiting connections is designed to be high, so they can emulate the behavior of the conventional connections under service-level loading conditions. However, the initial stiffness of the force-limiting connections is still lower than the stiffness of the conventional connections. As a result, the initial second-mode periods of the building models with force-limiting connections are longer than the ones for the building models with conventional connections. This effect is more pronounced when the lateral stiffness of the SFRS is higher, as can be checked in Figure 12B.

Figure 12B shows that the second-mode period of the building model with conventional connections using the Lumped-plasticity SFRS model is approximately constant during the ground motion. This is because this building model lacks the ability to modify the state of the lateral stiffness over the height of the building model during the ground motion excitation. This ability is in fact a key property introduced by the force-limiting connections that allows the mitigation of the contribution of the higher-mode response to the total seismic response of the building system. This property is attributed to the controlled inelastic force-displacement response of the force-limiting connections distributed over the height of the building. Figure 12B shows the considerable second-mode period elongation of the building models with force-limiting connections during the strong motion response. Figure 12A shows that the inelastic response of the force-limiting connections during the strong motion elongates the instantaneous second-mode periods of the building models to a range of lower spectral response accelerations, mitigating the contribution of the second-mode responses to the total seismic responses of the building models.

Figures 10D, 10H, and Table 6 show that the mean values and the corresponding dispersion of the peak SFRS story drift and connection deformation responses of the building models with conventional connections and force-limiting connections, respectively, are not significantly affected by the change in the SFRS modeling approach. Noticeable differences in the mean values of the peak SFRS story drift responses due to the change in the SFRS modeling approach are observed at the two lower stories; however, the mean values of these peak responses are smaller than the maximum mean values located at the 12^{th} story. Noticeable differences in the mean values of the connection deformation responses due to the change in the SFRS modeling approach are observed at the two higher floor levels; however, the mean values of these peak responses are smaller than the maximum mean values located at the third floor.

Figures 10E, 10F, and Table 6 show that the use of force-limiting connections instead of conventional connections reduces the mean values of the peak SFRS confined concrete minimum strain and SFRS reinforcing steel maximum strain amplitude responses at the base without affecting the dispersion of these peak responses.

The results of the numerical earthquake simulations indicate that the relative effects of the two studied SFRS modeling approaches on the acceleration and force responses of the building models are reduced by including force-limiting connections. This lower sensitivity to the SFRS modeling approach for the building models with force-limiting connections provides more confidence in the prediction of the seismic responses of these building systems. It is also verified that the magnitude and variability of the acceleration and force responses and the contribution of the higher-mode responses to the total seismic responses of the building models are reduced by including force-limiting connections. These results are consistent with conclusions given in previous research.[16,22]

5.3 | Effect of the uncertainty in the SFRS model parameters

The calibration process of the SFRS presented in Section 3.3.2 shows that the model parameters of the constitutive law used to simulate the response of the longitudinal reinforcing steel in the flexure-dominant inelastic base-mechanism RC walls have an important effect on the cyclic response of the walls. Therefore, it is expected that the uncertainty of these model parameters affects the seismic responses of the 12-story building models. The results presented in Sections 5.1 and 5.2 are obtained using the deterministic values of the steel model parameters given in Table 3. In this section, the steel model parameters are considered as uncertain to investigate the effects of their uncertainty on the variability of the distributions of the mean values of the peak seismic responses of the 12-story building models with conventional connections and force-limiting connections, respectively, subjected to design-basis intensity-level ground motions. The histograms of the mean values of the peak responses are compared with some reference values associated with seismic design and performance assessment of buildings.

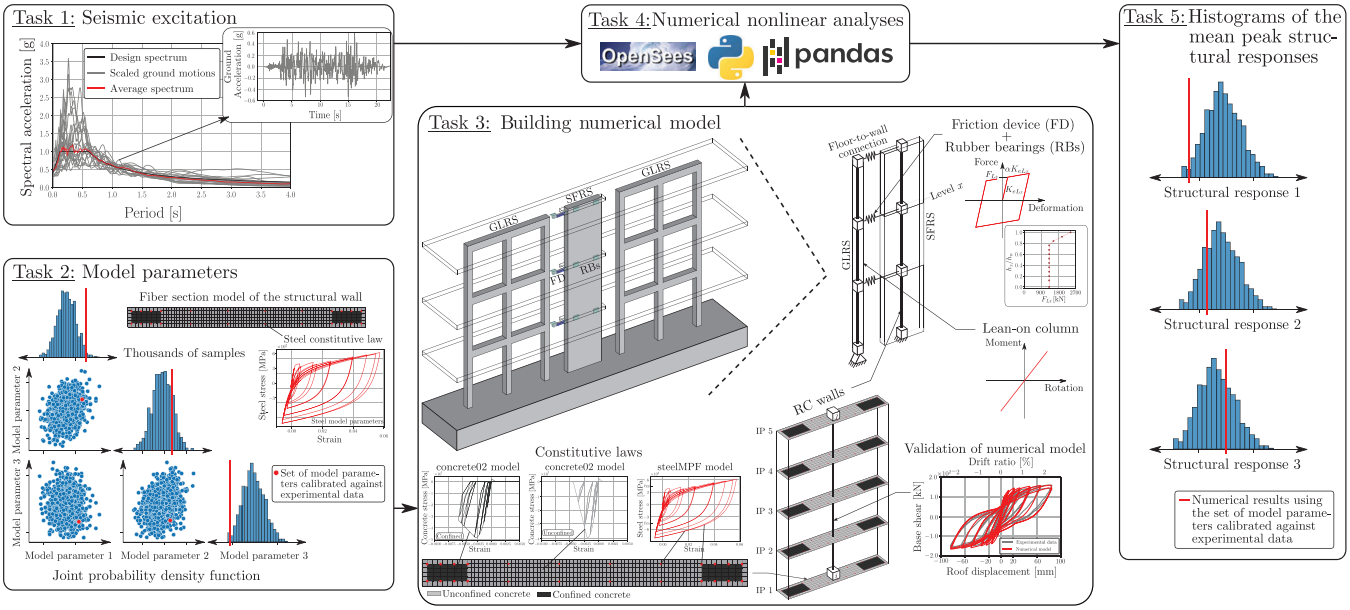

FIGURE 13 Flowchart of the uncertainty propagation analysis.

5.3.1 | Importance of uncertainty quantification

The quantification of the uncertainty in the model parameters is of paramount importance, particularly during sensitivity and reliability analyses in the context of seismic performance-based design and assessment of buildings. These analyses can expose the numerical models to conditions that may differ from those considered during the calibration of the numerical models.[43] Hence, it becomes imperative to comprehensively address and quantify the uncertainty in the model parameters to ensure accurate and reliable results.[44] The quantification of this uncertainty serves as a metric of the level of confidence in the seismic structural responses of buildings obtained from the numerical models. The level of confidence in the seismic structural responses is directly related to the level of confidence in the results of seismic performance-based design and assessment of buildings.

Previous research has quantified the uncertainty in the model parameters by performing uncertainty propagation, sensitivity, Bayesian model updating, or reliability analyses to assess the effects of the uncertainty in the model parameters on the seismic response and performance of structures.[43,45–50] They have explicitly considered the uncertainty in the model parameters by modeling it through suitable PDFs. They have demonstrated that considering this source of uncertainty introduces significant variability in the results of the seismic performance-based design and assessment of structures. This evidences the importance of considering this source of uncertainty when the performance of structures is assessed.

5.3.2 | Uncertainty propagation analysis

Figure 13 presents a flowchart that schematizes the tasks involved in the uncertainty propagation analysis conducted through Monte Carlo simulation. The tasks are: Task 1: Select a set of ground motions that are scaled to simulate design-basis intensity-level earthquakes, Task 2: Sample the model parameters considered as uncertain from the joint PDF, Task 3: Evaluate the building numerical model at each sample of the model parameters considered as uncertain, Task 4: Perform numerical nonlinear earthquake simulations of the building numerical models evaluated at each sample of the model parameters considered as uncertain subjected to the selected set of ground motions, and Task 5: Plot the histograms of the mean values of the peak structural responses of the building numerical models. This uncertainty propagation analysis is computationally expensive because of the large number of nonlinear numerical earthquake simulations required to obtain the results.

The joint PDF of the parameters of the Giuffrè-Menegotto-Pinto model presented in Table 2 is used to generate 4000 samples in the steel model parameter space. The building models are evaluated at each steel model parameter sample

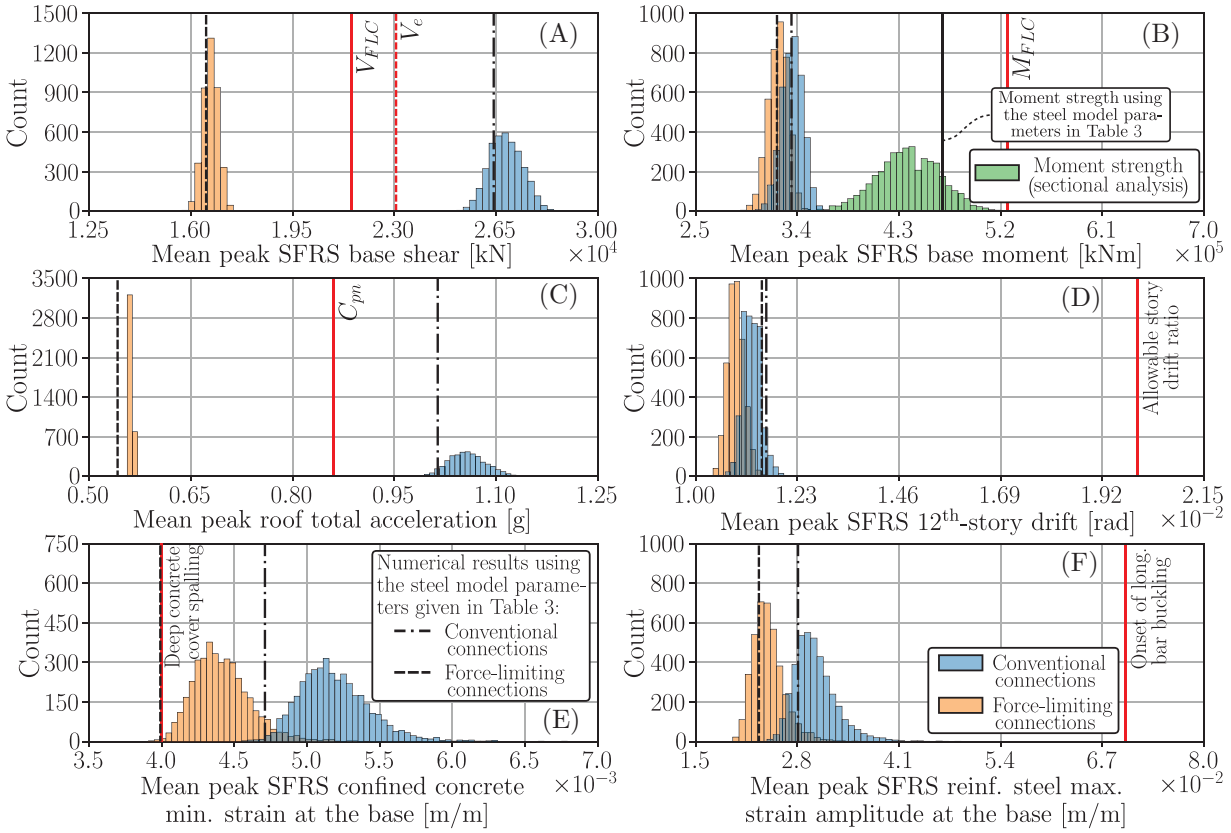

FIGURE 14 Histograms of the mean values of the peak SFRS base shear, SFRS base moment, roof total acceleration, SFRS 12th-story drift, SFRS confined concrete minimum strain at the base, and SFRS reinforcing steel maximum strain amplitude at the base responses from the 18 design-basis intensity-level ground motions. Twelve-story building models with conventional connections and force-limiting connections, respectively, using the Lean-on-column GLRS model and the Fiber-based SFRS model.

and subjected to the 18 design-basis intensity-level ground motions given in Section 4. Hence, 72,000 nonlinear dynamic analyses per connection case are performed in *OpenSees*[24] using parallel computation in *Python*.[51]

5.3.3 | Effects on the distributions of structural responses

Histograms of the mean values of the peak SFRS base shear, SFRS base moment, roof total acceleration, SFRS 12th-story drift, SFRS confined concrete minimum strain at the base, and SFRS reinforcing steel maximum strain amplitude at the base responses of the 12-story building models with conventional connections and force-limiting connections, respectively, subjected to the 18 design-basis intensity-level ground motions are presented in Figure 14. The mean values, standard deviations, and coefficients of variation of the resulting distributions of these mean peak seismic responses are listed in Table 7. Additionally, the peak seismic responses obtained in Section 5.2 using the deterministic steel model parameters given in Table 3 are presented as vertical black lines. The dashed-dotted lines correspond to building models with conventional connections and dashed lines correspond to building models with force-limiting connections. Some reference values associated with seismic design and performance assessment of buildings are presented as vertical red lines.

Figure 14A shows that the distributions of the mean peak SFRS base shear responses are significantly affected by the change in the GLRS-to-SFRS connections. The mean values and standard deviations of these distributions are reduced by more than 35.0% and 50.0%, respectively, by including force-limiting connections. The design base shear force V_e = 23059.9 kN[32] computed following the prescriptive seismic design for buildings with conventional connections is shown as a vertical red dashed line in Figure 14A. The mean peak SFRS base shear responses of the building models with conventional connections exceed V_e, whereas these mean peak responses for the building models with force-limiting connections are considerably smaller than V_e. The base shear V_{FLC} = 21543.5 kN computed as the sum of the design forces of the force-limiting connections over the height of the building is shown as a vertical red solid line in Figure 14A.

TABLE 7 Statistics of the distributions of the mean values of the peak seismic responses presented in Figure 14.

Response	Unit	GLRS-to-SFRS connection	Mean value	Standard deviation	Coefficient of variation
Mean peak SFRS base shear	kN	Conventional	26836.2	559.7	2.1%
		Force-limiting	16682.1	260.2	1.6%
Mean peak SFRS base moment	kNm	Conventional	335503.8	9429.2	2.8%
		Force-limiting	323121.4	8747.4	2.7%
Mean peak roof total acceleration	g	Conventional	1.058	0.0273	2.6%
		Force-limiting	0.563	0.0014	0.2%
Mean peak SFRS 12^{th}-story drift	rad	Conventional	0.0113	0.00020	1.8%
		Force-limiting	0.0109	0.00018	1.7%
Mean peak SFRS confined concrete minimum strain at the base	m/m	Conventional	0.00519	0.00026	5.0%
		Force-limiting	0.00442	0.00021	4.8%
Mean peak SFRS reinforcing steel max. strain amplitude at the base	m/m	Conventional	0.0304	0.00298	9.8%
		Force-limiting	0.0244	0.00213	8.7%

The mean peak SFRS base shear responses of the building models with force-limiting connections do not exceed V_{FLC}. This is expected because V_{FLC} can be considered an extreme value for the SFRS base shear response assuming that all force-limiting connections are activated simultaneously.

Figure 14B shows that the distributions of the mean peak SFRS base moment responses are not practically affected by the change in the GLRS-to-SFRS connections. These distributions resulted in similar mean values and standard deviations for the building models with conventional connections and force-limiting connections, respectively (see Table 7). This is expected because the RC walls that constitute the SFRS are designed to develop a ductile flexural inelastic base mechanism that limits the SFRS base moment responses. The ductile flexural inelastic base mechanism is designed to have an intended design moment strength and curvature capacity depending on the material properties, distribution of longitudinal reinforcing steel, and detailing of transverse confining steel. The SFRS base moment strength computed through sectional analysis also depends on the steel model parameters. The simulated samples of the steel model parameters from the joint PDF are used to obtain the distribution of the SFRS base moment strengths shown in Figure 14B. It is observed that some of the mean peak SFRS base moment responses of the building models with conventional connections exceed some of the SFRS base moment strengths, whereas these mean peak responses for the building models with force-limiting connections are smaller than the SFRS base moment strengths. The base moment $M_{FLC} = 526162.9$ kNm resulting from the distribution of the design forces of the force-limiting connections over the height of the building is shown as a vertical red line in Figure 14B. M_{FLC} can be considered an extreme value for the SFRS base moment response assuming that all force-limiting connections are activated simultaneously.

Figure 14C shows that the distributions of the mean peak roof total acceleration responses are significantly affected by the change in the GLRS-to-SFRS connections. The mean values and standard deviations of these distributions are reduced by more than 45.0% and 90.0%, respectively, by including force-limiting connections. As a reference value, the design acceleration coefficient C_{pn}, given by the Alternative Design Provisions for Diaphragms, including Chords and Collections per ASCE/SEI 7-22 Section 12.10.3,[31] is shown as a vertical red line in Figure 14C. Note that the mean peak roof total acceleration responses of the building models with conventional connections exceed C_{pn}, whereas these mean peak responses for the building models with force-limiting connections are considerably lower than C_{pn}. The deterministic values of the mean peak roof total acceleration responses from Section 5.2 are mostly exceeded by the mean peak roof total acceleration responses of the building models with conventional connections and force-limiting connections, respectively.

Figure 14D shows that the distributions of the mean peak SFRS 12^{th}-story drift responses are practically not affected by the change in the GLRS-to-SFRS connections. These distributions resulted in similar mean values and standard deviations for the building models with conventional connections and force-limiting connections, respectively (see Table 7). The mean peak SFRS 12^{th}-story drift responses of the building models with conventional connections and force-limiting connections, respectively, are significantly lower than the design limit of 0.020 rad,[31] shown as a vertical red line in Figure 14D. Therefore, no significant deformation at the design earthquake-intensity level is expected for the studied building with and without force-limiting connections.

Figure 14E shows that the distributions of the mean peak SFRS confined concrete minimum strain responses at the base are affected by the change in the GLRS-to-SFRS connections. The mean values and standard deviations of these distributions are reduced by 14.8% and 19.2%, respectively, by including force-limiting connections. All the mean peak SFRS confined concrete minimum strain responses at the base of the building models with conventional connections exceed the deep spalling limit state of 0.004 m/m,[52] shown as a vertical red line in Figure 14E. The deterministic value of the mean peak SFRS confined concrete minimum strain response at the base from Section 5.2 for the building model with force-limiting connections does not exceed the deep spalling limit state. Despite this, most of the mean peak SFRS confined concrete minimum strain responses at the base of the building models with force-limiting connections exceed the deep spalling limit state. These results show how important it is to consider the uncertainty in the steel model parameters when the seismic responses of the building models at fiber level are compared to limit states used in performance-based seismic design and assessment of buildings.

Figure 14F shows that the distributions of the mean peak reinforcing steel maximum strain amplitude responses at the base are affected by the change in the GLRS-to-SFRS connections. The mean values and standard deviations of these distributions are reduced by 19.7% and 28.5%, respectively, by including force-limiting connections. As expected, the uncertainty in the steel model parameters has a higher relative effect on the mean peak SFRS reinforcing steel maximum strain amplitude responses at the base than on the other studied mean peak responses. The coefficients of variation of the distributions of these mean peak responses are 9.8% and 8.7% for the building models with conventional connections and force-limiting connections, respectively. The mean peak SFRS reinforcing steel maximum strain amplitude responses at the base are considerably smaller than the onset of the longitudinal reinforcing steel bar buckling limit state of 0.070 m/m,[53] shown as a vertical red line in Figure 14F.

The use of force-limiting connections between the GLRS and the SFRS not only reduces the mean values of the distributions of the mean peak SFRS base shear, roof total acceleration, SFRS confined concrete minimum strain at the base, and SFRS reinforcing steel maximum strain amplitude at the base responses but also reduces the dispersion of these distributions due to the uncertainty in the steel model parameters. This effect is more pronounced on the distributions of the mean peak SFRS base shear and roof total acceleration responses. The resulting distributions of the mean peak SFRS confined concrete minimum strain responses at the base demonstrated that not considering the uncertainty in the steel model parameters can lead to unconservative estimates of the seismic responses used to check the design limit states. The reduction in the dispersion of the distributions of the structural responses by including force-limiting connections gives higher confidence in the seismic response prediction, which can be reflected in higher confidence in the performance-based seismic design and assessment of buildings with force-limiting connections.

6 | SUMMARY

This paper assessed the effects of (1) the GLRS modeling approach, (2) the SFRS modeling approach, and (3) the uncertainty of the model parameters of the constitutive law of the longitudinal reinforcing steel of the SFRS on the simulated seismic responses of a 12-story RC building with force-limiting connections. This was achieved by conducting nonlinear numerical simulations of building models subjected to a set of far-field ground motions scaled to the design-basis intensity-level earthquake. First, the seismic responses of the building models with force-limiting connections using two GLRS modeling approaches, (1) a moment frame system (Moment-frame model) and (2) a pin-base lean-on-column system (Lean-on-column model), were compared. Then, the seismic responses of the building models with conventional connections and force-limiting connections, respectively, using two SFRS modeling approaches, (1) a distributed-plasticity modeling approach (Fiber-based model) and (2) a lumped-plasticity modeling approach (Lumped-plasticity model), were compared. The model parameters of the Fiber-based model were calibrated and validated against experimental test results available in the literature. The joint PDF for the ASTM-A615 Grade 60 steel proposed by Birrell et al.[30] provided the expected ranges of variation of the model parameters of the constitutive law of the longitudinal reinforcing steel fibers used for calibration. Finally, the joint PDF of the steel model parameters was used to conduct an uncertainty propagation analysis through Monte Carlo earthquake simulation. The uncertainty in the steel model parameters was propagated to the seismic responses of the building models with conventional connections and force-limiting connections, respectively. The distributions of the mean values of the peak structural responses of the building models were studied. Additionally, this paper verified that the use of force-limiting connections instead of conventional connections reduces the magnitude and variability of the acceleration and force responses and the higher-mode response contributions to the seismic responses of the building models.

7 | CONCLUSIONS

- The joint PDFs of numerical model parameters based on experimental test results give valuable information on the expected values and ranges of variation of the model parameters that can be used for calibration and validation of nonlinear models for numerical earthquake simulation.
- The mean values and dispersion of the peak SFRS and GLRS-to-SFRS connection responses of the 12-story building models with force-limiting connections are not practically affected by the GLRS modeling approach.
- The use of force-limiting connections between the GLRS and the SFRS considerably reduces the effects of the SFRS modeling approach on the mean values and dispersion of the peak SFRS story shear, SFRS moment, floor total acceleration, and GLRS-to-SFRS connection force responses.
- The cracking evolution over the height of the RC walls modifies the state of the stiffness over the height of the building models and, as a result, it reduces the contribution of the second-mode responses to the total seismic responses of the building models. The use of force-limiting connections between the GLRS and the SFRS allows for further modification of the state of the stiffness over the height of the building models; therefore, a higher reduction of the contribution of the second-mode responses is achieved.
- The use of force-limiting connections between the GLRS and the SFRS not only reduces the mean values of the distributions of the mean peak SFRS base shear, roof total acceleration, SFRS confined concrete minimum strain at the base, and SFRS reinforcing steel maximum strain amplitude at the base responses but also reduces the dispersion of these distributions due to the uncertainty in the steel model parameters. This effect is more pronounced on the distributions of the mean peak SFRS base shear and roof total acceleration responses.
- The uncertainty in the steel model parameters considerably affects the distributions of the mean peak SFRS confined concrete minimum strain and SFRS reinforcing steel maximum strain amplitude responses at the base of the 12-story building models. Not considering this source of uncertainty can lead to unconservative estimates of the seismic responses used to check design limit states.

The reduction in the effects of the modeling approaches of the structural components on the seismic responses of the building models by including force-limiting connections between the GLRS and the SFRS gives higher confidence in the prediction of the seismic responses, which can be reflected in higher confidence in the performance-based seismic design and assessment of buildings with force-limiting connections.

AUTHOR CONTRIBUTIONS

C. Franco Mayorga conceived the research project; conducted a literature review; conducted the numerical earthquake simulations; prepared figures and diagrams; interpreted the numerical results; and wrote the manuscript. **Georgios Tsampras** conceived the research project; conducted a literature review; provided critical guidance throughout the research process; contributed to the interpretation of the results; and co-wrote and revised the manuscript.

ACKNOWLEDGMENTS

The authors acknowledge the Department of Structural Engineering at the University of California San Diego (UCSD), the American Concrete Institute (ACI) Foundation, and the Chilean National Agency for Research and Development (ANID) for their financial support. Additionally, the authors would like to express their sincere gratitude to Kyoungyeon Lee and Kaixin Chen for their invaluable support throughout the development of this research project. Any opinions, findings, and conclusions expressed in this paper are those of the authors and do not necessarily reflect the views of others acknowledged here.

CONFLICT OF INTEREST STATEMENT

The authors declare no potential conflict of interest.

DATA AVAILABILITY STATEMENT

The data that support the findings of this study are available from the corresponding author upon reasonable request.

ORCID

C. Franco Mayorga https://orcid.org/0009-0009-2471-5207
Georgios Tsampras https://orcid.org/0000-0001-8255-3415

REFERENCES

1. Esmaeiltabar P, Vaseghi J, Khosravi H. Nonlinear Macro modeling of slender reinforced concrete shear walls. *Struct Concr*. 2019;20(3):899-910. doi:10.1002/suco.201800206
2. Orakcal K, Massone LM, Wallace JW. *Analytical Modeling of Reinforced Concrete Walls for Predicting Flexural and Coupled–Shear-Flexural Responses PEER 2006/07 Report*. tech. rep., Pacific Earthquake Engineering Research Center; 2006.
3. Taucer F, Spacone E, Filippou F. *A Fiber Beam-Column Element for Seismic Response Analysis of Reinforced Concrete Structures UCB/EERC-91/17 Report*. tech. rep., Earthquake Engineering Research Center College of Engineering University of California; 1991.
4. Panagiotou M, Restrepo JI, Schoettler M, Kim G. Nonlinear cyclic truss model for reinforced concrete walls. *Struct J*. 2012;109(2):205-214. doi:10.14359/51683631
5. Pozo JD, Hube MA, Kurama YC. Effective nonlinear simulations of RC columns with force-based elements. *J Earthquake Eng*. 2023;27(2):340-361. doi:10.1080/13632469.2021.2001395
6. Kolozvari K, Arteta C, Fischinger M, et al. Comparative study of state-of-the-art macroscopic models for planar reinforced concrete walls. *ACI Struct J*. 2018;115(6):1637-1657. doi:10.14359/51710835
7. Pozo JD, Hube MA, Kurama YC. Quantification of variability in simulated seismic performance of RC wall buildings. *Eng Struct*. 2023;295:116872. doi:10.1016/j.engstruct.2023.116872
8. Belletti B, Damoni C, Gasperi A. Modeling approaches suitable for pushover analyses of RC structural wall buildings. *Eng Struct*. 2013;57:327-338. doi:10.1016/j.engstruct.2013.09.023
9. Pozo JD, Hube MA, Kurama YC. Quantitative assessment of nonlinear macro-models for global behavior and design of planar RC walls. *Eng Struct*. 2020;224:111190. doi:10.1016/j.engstruct.2020.111190
10. Lu Y, Panagiotou M, Koutromanos I. Three-dimensional beam-truss model for reinforced concrete walls and slabs – Part 1: Modeling approach, validation, and parametric study for individual reinforced concrete walls. *Earthquake Eng Struct Dyn*. 2016;45(9):1495-1513. doi:10.1002/eqe.2719
11. Lu Y, Panagiotou M. Three-dimensional beam– truss model for reinforced concrete walls and slabs – Part 2: Modeling approach and validation for slabs and coupled walls. *Earthquake Eng Struct Dyn*. 2016;45(11):1707-1724. doi:10.1002/eqe.2720
12. Mavros M, Panagiotou M, Koutromanos I, Alvarez R, Restrepo JI. Seismic analysis of a modern 14-story rein forced concrete core wall building system using the BTM-shell methodology. *Earthquake Eng Struct Dyn*. 2022;51(6):1540-1562. doi:10.1002/eqe.3627
13. Fleischman RB, Farrow KT. Dynamic behavior of perimeter lateral-system structures with flexible diaphragms. *Earthquake Eng Struct Dyn*. 2001;30(5):745-763. doi:10.1002/eqe.36
14. Rodriguez ME, Restrepo JI, Carr AJ. Earthquake-induced floor horizontal accelerations in buildings. *Earthquake Eng Struct Dyn*. 2002;31(3):693-718. doi:10.1002/eqe.149
15. Rodriguez ME, Restrepo JI, Blandón JJ. Seismic design forces for rigid floor diaphragms in precast concrete building structures. *J Struct Eng*. 2007;133(11):1604-1615. doi:10.1061/(ASCE)0733-9445(2007)133:11(1604)
16. Tsampras G, Sause R, Zhang D, et al. Development of deformable connection for earthquake-resistant buildings to reduce floor accelerations and force responses. *Earthquake Eng Struct Dyn*. 2016;45(9):1473-1494. doi:10.1002/eqe.2718
17. Tsampras G. *Force-Limiting Floor Diaphragm Connection for Earthquake-Resistant Buildings*. PhD thesis. Lehigh University; 2016.
18. Tsampras G, Sause R, Fleischman RB, Restrepo JI. Experimental study of deformable connection consisting of buckling-restrained brace and rubber bearings to connect floor system to lateral force resisting system. *Earthquake Eng Struct Dyn*. 2017;46(8):1287-1305. doi:10.1002/eqe.2856
19. Tsampras G, Sause R, Fleischman RB, Restrepo JI. Experimental study of deformable connection consisting of friction device and rubber bearings to connect floor system to lateral force resisting system. *Earthquake Eng Struct Dyn*. 2018;47(4):1032-1053. doi:10.1002/eqe.3004
20. Zhang Z, Fleischman RB, Restrepo JI, et al. Shake-table test performance of an inertial force-limiting floor anchorage system. *Earthquake Eng Struct Dyn*. 2018;47(10):1987-2011. doi:10.1002/eqe.3047
21. Paronesso M, Lignos DG. Experimental study of sliding friction damper with composite materials for earthquake resistant structures. *Eng Struct*. 2021;248:113063. doi:10.1016/j.engstruct.2021.113063
22. Tsampras G, Sause R. Force-based design method for force-limiting deformable connections in earthquake-resistant buildings. *J Struct Eng*. 2022;148(10):04022150. doi:10.1061/(ASCE)ST.1943-541X.0003456
23. Paronesso M, Lignos DG. Seismic design and performance of steel concentrically braced frame buildings with dissipative floor connectors. *Earthquake Eng Struct Dyn*. 2022;51(15):3505-3525. doi:10.1002/eqe.3733
24. McKenna F, Scott MH, Fenves GL. Nonlinear finite-element analysis software architecture using object composition. *J Comput Civ Eng*. 2010;24(1):95-107.doi:10.1061/(ASCE)CP.1943-5487.0000002
25. Mayorga CF, Lee K, Tsampras G. Effect of the structural wall modeling in the seismic response of buildings with force-limiting connections between diaphragm-to-wall joints. Abstract presented at: Engineering Mechanics Institute (EMI) Conference 2022; May 31–June 3, 2022; Baltimore, MD. Session M306.
26. Thomsen JH, Wallace JW. *Displacement-Based Design of RC Structural Walls: An Experimental Investigation of Walls with Rectangular and T-shaped Cross-sections*. Clarkson University, Department of Civil Engineering; 1995.
27. Elwood K. *University of Auckland High Axial Load Wall Tests*. DesignSafe-CI Type; 2018. dataset doi:10.17603/DS2609N
28. Wallace J, Arteta C, Segura C. *NEESR: Seismic Performance of Conventional and Innovative Special Structural Walls*. DesignSafe-CI Type; 2018. dataset doi:10.17603/DS2P41P

29. Menegotto M, Pinto PE. Method of Analysis for Cyclic Loaded R. C. Plane frame including changes in geometry and non-elastic behaviour of elements under combined normal force and bending. *Proceedings of IABSE Symposium on Resistance and Ultimate Deform ability of Structures Acted On by Well Defined Repeated Loads*. 1973;11:15-22. doi:10.5169/seals-13741
30. Birrell M, Astroza R, Carreño R, Restrepo JI, Araya-Letelier G. Bayesian parameter and joint probability distribution estimation for a hysteretic constitutive model of reinforcing steel. *Struct Saf*. 2021;90:102062. doi:10.1016/j.strusafe.2020.102062
31. ASCE/SEI 7-22. *Minimum Design Loads and Associated Criteria for Buildings and Other Structures*. American Society of Civil Engineers; 2021.
32. Committee 318 American Concrete Institute. *Building Code Requirements for Structural Concrete (ACI 318-19): An ACI Standard; Commentary on Building Code Requirements for Structural Concrete (ACI 318R-19)*. American Concrete Institute; 2019.
33. FEMA P-1050-1. *NEHRP Recommended Seismic Provisions for New Buildings and Other Structures*. FEMA; 2015.
34. Mohd Yassin MH. *Nonlinear Analysis of Prestressed Concrete Structures under Monotonic and Cyclic Loads*. PhD thesis. University of California; 1994.
35. Filippou F, Popov E, Bertero V. Effects of Bond Deterioration on Hysteretic Behavior of Reinforced Concrete Joints. UCB/EERC-83/19 Report. tech. rep., Earthquake Engineering Research Center; 1983.
36. Coleman J, Spacone E. Localization issues in force-based frame elements. *J Struct Eng*. 2001;127(11):1257-1265. doi:10.1061/(ASCE)0733-9445(2001)127:11(1257)
37. Committee 224 American Concrete Institute. *Control of Cracking in Concrete Structures (ACI-224-01)*. American Concrete Institute; 2001.
38. Moehle J. *Seismic Design of Reinforced Concrete Buildings*. McGraw-Hill Education; 2014.
39. Mander JB, Priestley MJN, Park R. Theoretical stress-strain model for confined concrete. *J Struct Eng*. 1988;114(8):1804-1826. doi:10.1061/(ASCE)0733-9445(1988)114:8(1804)
40. Lowes LN, Mitra N, Altoontash A. A Beam-Column Joint Model for Simulating the Earthquake Response of Reinforced Concrete Frames. PEER 2003/10 Report. tech. rep., Pacific Earthquake Engineering Research Center; 2003.
41. FEMA P-695. *Quantification of Building Seismic Performance Factors*. FEMA; 2009.
42. Baker JW. Conditional mean spectrum: tool for ground-motion selection. *J Struct Eng*. 2011;137(3):322-331. doi:10.1061/(ASCE)ST.1943-541X.0000215
43. Deb A, Zha AL, Caamaño-Withall ZA, Conte JP, Restrepo JI. Simplified risk-targeted performance-based seismic design method for ordinary standard bridges. *J Bridge Eng*. 2022;27(10):04022089. doi:10.1061/(ASCE)BE.1943-5592.0001916
44. Schuëller GI. On the treatment of uncertainties in structural mechanics and analysis. *Comput Struct*. 2007;85(5):235-243. doi:10.1016/j.compstruc.2006.10.009
45. Jensen HA, Mayorga F, Valdebenito M, Chen J. An effective parametric model reduction technique for uncertainty propagation analysis in structural dynamics. *Reliab Eng Syst Saf*. 2020;195:106723. doi:10.1016/j.ress.2019.106723
46. Astudillo B, Rivera D, Duke J, et al. Modeling uncertainty of specimens employing spines and force-limiting connections tested at E-defense shake table. *Earthquake Eng Struct Dyn*. 2023;52:4638-4659. doi:10.1002/eqe.3976
47. Grandhi RV, Fischer CC. Model-form uncertainty quantification for structural design. In: Beer M, Kougioumtzoglou IA, Patelli E, Au ISK, eds. *Encyclopedia of Earthquake Engineering*. Springer; 2014:1-17.
48. Ramancha MK, Conte JP, Parno MD. Accounting for model form uncertainty in Bayesian calibration of linear dynamic systems. *Mech Syst Sig Process*. 2022;171:108871. doi:10.1016/j.ymssp.2022.108871
49. Jensen HA, Mayorga F, Valdebenito MA. On the reliability of structures equipped with a class of friction-based devices under stochastic excitation. *Comput Meth Appl Mech Eng*. 2020;364:112965. doi:10.1016/j.cma.2020.112965
50. Deb A, Conte JP, Restrepo JI. Comprehensive treatment of uncertainties in risk-targeted performance-based seismic design and assessment of bridges. *Earthquake Eng Struct Dyn*. 2022;51(14):3272-3295. doi:10.1002/eqe.3722
51. Van Rossum G, Drake FL. *Python 3 Reference Manual*. CreateSpace; 2009.
52. Kent DC, Park R. Flexural members with confined concrete. *J Struct Div*. 1971;97(7):1969-1990. doi:10.1061/JSDEAG.0002957
53. Rodriguez ME, Botero JC, Villa J. Cyclic stress-strain behavior of reinforcing steel including effect of buckling. *J Struct Eng*. 1999;125(6):605-612. doi:10.1061/(ASCE)0733-9445(1999)125:6(605)

How to cite this article: Mayorga CF, Tsampras G. Reinforced concrete wall buildings with force-limiting connections: Modeling effects and uncertainty propagation. *Earthquake Engng Struct Dyn*. 2024;1-27. https://doi.org/10.1002/eqe.4073